

## SCALING THE RESPONSE OF DELTAS TO RELATIVE-SEA-LEVEL CYCLES BY AUTOGENIC SPACE AND TIME SCALES: A LABORATORY STUDY

LIZHU YU, QI LI,\* AND KYLE M. STRAUB

*Department of Earth and Environmental Sciences, Tulane University, New Orleans, Louisiana 70118, U.S.A.  
e-mail: kmstraub@tulane.edu*

**ABSTRACT:** Relative-sea-level (RSL) change influences surface processes and stratigraphic architecture of deltaic systems and has been studied extensively for decades. However, we still lack a quantitative framework to define how the magnitude and period of a RSL cycle influences deltaic morphodynamics and the resulting stratigraphy. One method for scaling the magnitude and period of RSL cycles is through comparison with the autogenic time and space scales that characterize individual deltaic systems. We explore this method using a suite of physical experiments that shared identical forcing conditions with the exception of sea level. This approach utilizes two nondimensional numbers that characterize the magnitude and period of RSL cycles. Magnitude is defined with respect to the maximum autogenic channel depth, while the period is defined with respect to the time required to deposit one channel depth of sediment, on average, everywhere in a basin. The experiments include: 1) a control experiment lacking RSL cycles, used to define autogenic scales, 2) a low-magnitude, long-period (LMLP) stage, and 3) a high-magnitude, short-period (HMSP) stage. We observe clear differences in the response of deltas to the forcing in each experiment. The RSL cycles in the HMSP stage induce allogenic surface processes and stratigraphic products with scales that exceed the stochastic variability found in the control stage. These include the generation of rough shorelines and long temporal gaps in the stratigraphy. In contrast, the imprint of LMLP cycles on surface processes and stratigraphy is found in properties that define the mean state of a system. These include the mean shoreline location and the timing and location of mass extraction from the transport system. This work demonstrates the effectiveness of defining the magnitude and period of RSL cycles through autogenic scales and provides insights for generation of forward stratigraphic models influenced by RSL change.

### INTRODUCTION

The influence of a receiving basin's water-surface elevation, either lake or sea level and commonly referred to as base level, on deltaic systems and their stratigraphic records is one of the most studied questions in all of sedimentary geology. Going back to the work of Gilbert (1890), a plethora of studies tackled this question using field observations (Vail et al. 1977; Van Wagoner et al. 1990; Blum and Törnqvist 2000; Anderson 2004; Bhattacharya 2011), numerical experiments (Flemings and Grotzinger 1996; Granjeon and Joseph 1999; Karssenbergh and Bridge 2008; Burgess and Prince 2015) and laboratory experiments (Koss et al. 1994; Heller et al. 2001; Van Heijst and Postma 2001; Martin et al. 2009; Li et al. 2016). This body of work has led to an entire branch of stratigraphy termed sequence stratigraphy (Vail et al. 1977; Van Wagoner et al. 1990; Catuneanu 2002; Zecchin and Catuneanu 2013). While much is now known about the influence of sea level on deltas (Blum and Törnqvist 2000; Heller et al. 2001; Catuneanu et al. 2009; Burgess and Prince 2015; Nijhuis et al. 2015), we still lack a quantitative framework to define how the magnitude and period of base-level cycles influence deltaic dynamics and their stratigraphic products for systems of various scales. Here we take a first pass at defining a normalized magnitude and period of base-level cycles, in

relation to the spatial and temporal scales of a delta's internal dynamics. We estimate these autogenic scales using parameters that can plausibly be measured for most field-scale systems. Our goal is to link these normalized variables to characteristic morphodynamic and stratigraphic attributes in an effort to improve forward stratigraphic prediction and inversion of the stratigraphic record.

In their seminal work on architecture of clastic sequences, Van Wagoner et al. (1990) define a hierarchy of scales for stratigraphic stacking patterns. Some of these scales, for example laminae and beds, are discussed as products of a system's internal dynamics. On the other end of the spectrum, some scales are purely associated with external forcings. In the middle of their hierarchy, though, are deposits referred to as parasequences, which are defined as relatively conformable successions of genetically related beds or bedsets bounded by marine flooding surfaces and their correlative surfaces which form over hundreds to tens of thousands of years with thicknesses between meters to hundreds of meters. Van Wagoner et al. (1990) state that these could be the product of both internal dynamics and external forcings. The competing influence of internal dynamics and external forcings for parasequence formation hints at certain spatial and temporal scales which could be used in comparison to characteristics of RSL cycles.

While early work on deltaic stratigraphy focused on external forcings, the last ten years has seen an explosion in the number of studies that focus

\* Present Address: Department of Earth and Environmental Sciences, Georgia Institute of Technology, Atlanta, Georgia 30332, U.S.A.

on the internal dynamics of deltaic systems and their stratigraphic products (Muto 2001; Hickson et al. 2005; Kim et al. 2006; Van Dijk et al. 2009; Wang et al. 2011; Karamitopoulos et al. 2014; Li et al. 2016). This has largely been led by results coming from experimentalists working with deltas produced in laboratory settings. The reason behind this is simple: experimental deltas with horizontal scales of meters constructed over tens to hundreds of hours allow researchers to directly observe a system's internal dynamics. Examples of these internal dynamics include bar migration, avulsions, and deltaic lobe switching. Physical experiments also allow researchers to explore the influence of boundary and forcing conditions, as these can be accurately controlled in laboratory settings. Observations from these experiments suggest that internal deltaic dynamics, often referred to as autogenics, can influence surface dynamics and stratigraphic records over much greater time scales than previously thought: tens of thousands to hundreds of thousands of years (Kim et al. 2006; Kim and Paola 2007; Wang et al. 2011). Motivated by these experimental observations, several recent studies used numerical experiments to isolate the influence of autogenic processes and support the influence of autogenics on stratigraphy out to time scales important to basin filling (Dalman et al. 2015; Liang et al. 2016). These physical and numerical experiments are starting to produce a reevaluation of field-scale stratigraphic architecture that incorporates autogenics in their interpretations (Hofmann et al. 2011; Hajek et al. 2012; Chamberlin and Hajek 2015).

Physical experiments have been used to study the influence of base-level cycles on stratigraphic architecture for some time now (Wood et al. 1993; Koss et al. 1994; Heller et al. 2001; Van Heijst and Postma 2001; Martin et al. 2009; Li et al. 2016). Here we highlight work by Heller et al. (2001) which examined the influence of "short" and "long" base-level cycles. In this study, performed in the eXperimental Earth-Scape (XES) basin, short and long were in reference to the equilibrium channel response time,  $T_{eq}$ , of the system to an external forcing.  $T_{eq}$  is defined by Paola et al. (1992) as the time associated with a basin evolving to the condition where subsidence and sedimentation are balanced, which scales as

$$T_{eq} \approx \frac{L^2}{\nu} \quad (1)$$

where  $L$  is the characteristic length of a system and  $\nu$  is a transport (diffusion) coefficient. Heller et al. (2001) found that when a base-level cycle was long in comparison to  $T_{eq}$ , systems tend to generate laterally extensive unconformities without the formation of valleys, whereas local unconformities and their paleo-valley fills were associated with base-level cycles that are short with respect to  $T_{eq}$ . While their study examined "short" and "long" base-level cycles, they did not examine the influence of the magnitude of a base-level cycle.

Recently, Li et al. (2016) examined the influence of both cycle magnitude and period on the storage of base-level information in stratigraphy. In their study, Li et al. (2016) define storage thresholds associated with the space and time scales of a system's autogenic processes. This allowed them to define cycle magnitude and period for systems of varying size through a comparison of the scale of the external forcing to the scale of the internal dynamics. The main thrust of the work of Li et al. was an examination of deposition-rate time series with the aim of defining thresholds for the storage of information pertaining to base-level changes in stratigraphy. Examination of power spectra of the deposition-rate time series supported the stratigraphic storage thresholds proposed by Li et al. However, more work is required to examine how morphodynamics respond to the magnitude and periodicity of sea-level cycles when scaled to autogenic processes and what this means for the resulting stratigraphy, including architectural scales and bulk volumetric attributes.

The goal of this study is to more fully characterize the surface processes and stratigraphic attributes associated with base-level cycles that are stored

due to either their large magnitude or long period. Specifically, we hypothesize 1) that base-level cycles with large magnitudes but short periods will induce cyclic morphodynamic responses and produce stratigraphic products with rates and architectural scales that exceed those found in systems with constant forcing; and 2) base-level cycles with long periods but small magnitudes will share process rates and stratigraphic architectural scales similar to those of systems with constant forcing. However, these cycles will influence mean attributes of the morphodynamics and store signals of RSL cycles in bulk characteristics of the stratigraphy, e.g., mean volumetric growth rates, and mean location of paleo-shoreline indicators, from those in systems with constant forcing.

## THEORY

Here we present theory to define the magnitude and period of relative-sea-level (RSL) cycles through a comparison of the scales of deltaic autogenic processes. Here RSL change is defined as the sum of local sea-level rise and subsidence rates. We define a nondimensional magnitude and period of sea-level change in the manner proposed by Li et al. (2016), which is represented here for completeness and clarity.

Starting with the magnitude of RSL cycles: we compare the range of a RSL cycle,  $M_{RSL}$ , (i.e., difference in elevation from cycle peak to trough) to the depth of the largest channels,  $H_c$ , that are observed in a system with constant boundary conditions:

$$H^* = \frac{M_{RSL}}{H_c} \quad (2)$$

We use  $H_c$  because the largest experimental autogenic elevation changes are associated with post-avulsion channel incision. We view  $H_c$  as a conservative upper estimate of autogenic elevation changes as some hypothesize that the generation of landforms such as alluvial ridges might actually lead to larger autogenic elevation changes in field systems (Trampush et al. 2017). Next we compare the period of a RSL cycle,  $T_{RSL}$ , to the maximum time scale of autogenics in deltaic systems. Wang et al. (2011) defined this as the compensation time,  $T_c$ , and showed that it scaled with the time necessary to deposit, on average, one channel depth of strata everywhere in a basin. In other words,  $T_c$ , represents the time necessary for a particle deposited at Earth's surface to be buried to a depth that is no longer susceptible to remobilization from autogenic incision events (Straub and Esposito 2013). This produces a nondimensional time that scales as

$$T^* = \frac{T_{RSL}}{T_c} \quad (3)$$

Combined,  $H^*$  and  $T^*$  provide a method to compare a normalized magnitude and period of RSL cycles to the morphodynamics of individual systems.

## EXPERIMENTAL METHODS

To study the influence of RSL cycles on surface processes and stratigraphic records we conduct a series of physical laboratory experiments in the Delta Basin at the Tulane University Sediment Dynamics and Stratigraphy Laboratory. This basin is 4.2 m long, 2.8 m wide, and 0.65 m deep (Fig. 1). Sea-level is controlled through a weir, which is in hydraulic communication with the basin. The weir is on a computer-controlled vertical slide that allows for sub-millimeter-scale elevation control of sea-level. The sea-level elevation was monitored and logged once a minute with a transducer to ensure that its elevation matched target elevations. Supply of water and sediment are also controlled through this computer interface and were kept at constant values of  $1.7 \times 10^{-4} \text{ m}^3/\text{s}$  and  $3.9 \times 10^{-4} \text{ kg/s}$ , respectively for each experiment.

We first performed a control experiment, TDB-12, with constant forcing conditions to define the autogenic time and space scales necessary to

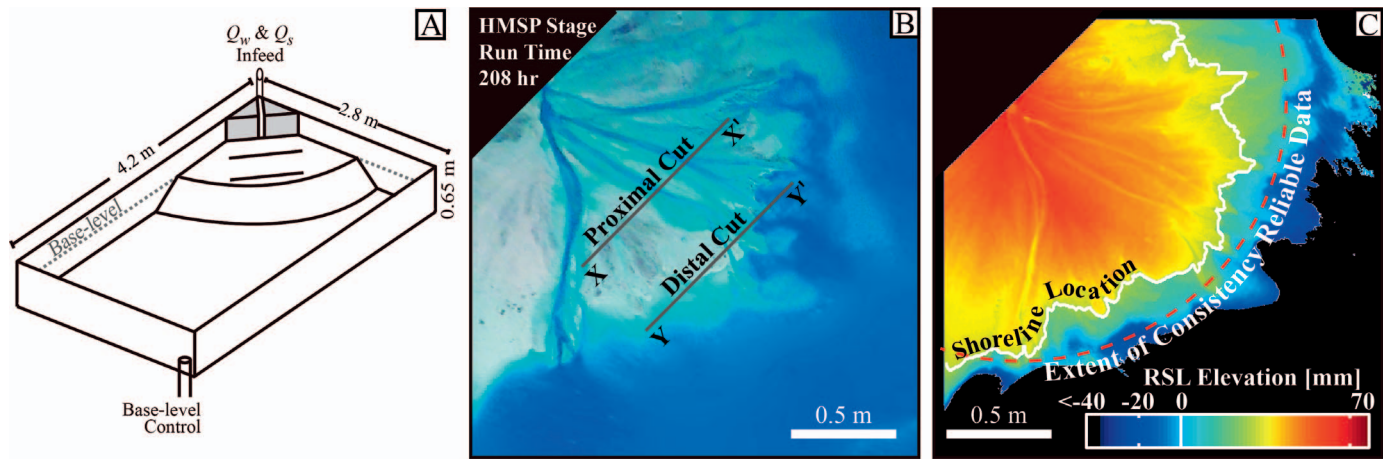


FIG. 1.—Schematic of experimental setup and maps illustrating types of data collected over the course of each experimental stage. **A)** Schematic diagram of Tulane Delta Basin with key basin dimensions and controls labeled. **B)** Characteristic digital image of the HMSCP stage with flow on and dyed for visualization. Image collected with laser scanner such that all pixels are referenced relative to the basin coordinate system. Locations of physical stratigraphic sections are shown by solid black lines. **C)** DEM of experimental surface collected with laser scanner. Solid white line denotes shoreline. Dashed red line shows the extent of DEMs where topography was reliably measured for each run hour.

calculate  $H^*$  and  $T^*$  (Fig. 2). These forcings include a constant rate of sea-level rise (or pseudo-subsidence),  $\bar{r}$ , equal to 0.25 mm/hr, that resulted in a nearly constant terrestrial accommodation production rate that matched the volumetric input rate of sediment to the experiment. We define terrestrial accommodation as the depth available for deposition below the theoretical long-term graded profile of a transport system (Mackin 1948; Vail 1987; Straub and Wang 2013). As a result, the mean location of the shoreline varied only due to autogenic processes during the course of the experiment. This experiment was run for 900 hr and resulted in a deposit thickness of approximately 225 mm. The input sediment mixture was designed to mimic earlier experimental work (Hoyal and Sheets 2009) with particle diameters ranging from 1 to 1000  $\mu\text{m}$  with a mean of 67  $\mu\text{m}$  and was dominantly white quartz. One quarter of the coarsest 23.5% of the distribution was commercially dyed to aid visualization of stratigraphic architecture. A small amount of commercially available polymer (New Drill Plus, distributed by Baker Hughes Inc.) was added to the sediment mixture to enhance sediment cohesion, which aids formation of channels in experiments (Hoyal and Sheets 2009). In all experiments discussed, the input water to the basin was dyed with a food coloring to aid characterization of morphodynamics. From this experiment we were able to define  $H_c$  as 12.25 mm and  $T_c$  as 49 hr.

Given the fact that we are using a long-term sea-level rise as a proxy for long-term subsidence in the basin, we must take care in defining certain terms. In our experiments changes in the elevation of sea level above the basin floor, resulting from the long-term sea-level rise and any superimposed cycles, is equivalent to relative-sea-level in field-scale systems (i.e., the sum of subsidence and eustatic sea level). As such, and for easier comparison with field systems, the elevation of sea level above the basin floor will be referred to as relative-sea-level (Fig. 2A). Next, we refer to eustatic sea level in our experiments as the elevation of sea level relative to the basin floor minus the long-term sea-level rise imposed to mimic subsidence. As such, the mean eustatic sea level in all experiments is 0, while positive values indicate highstands and negative values indicate lowstands (Fig. 2B).

Next we performed experiment TDB-15-1, designed to isolate the influence of cycle magnitude and period on deltaic morphodynamics and stratigraphy. TDB-15-1 had forcing conditions identical to those detailed for TDB-12, with the exception of RSL cycles that varied in magnitude and period. The shape of the cycles were defined by a sine wave, which is a simplification of Milankovitch cycles, whose shape depends on a number

of climatic and paleo-geographic parameters (Miller et al. 2005). The first stage of TDB-15-1 had RSL cycles defined by  $H^* = 0.5$  and  $T^* = 2$ , while the second stage had RSL cycles defined by  $H^* = 2.0$  and  $T^* = 0.5$  (Fig. 2). We will refer to the first stage as the low-magnitude long-period (LMLP) stage, and the second stage as the high-magnitude short-period (HMSCP)

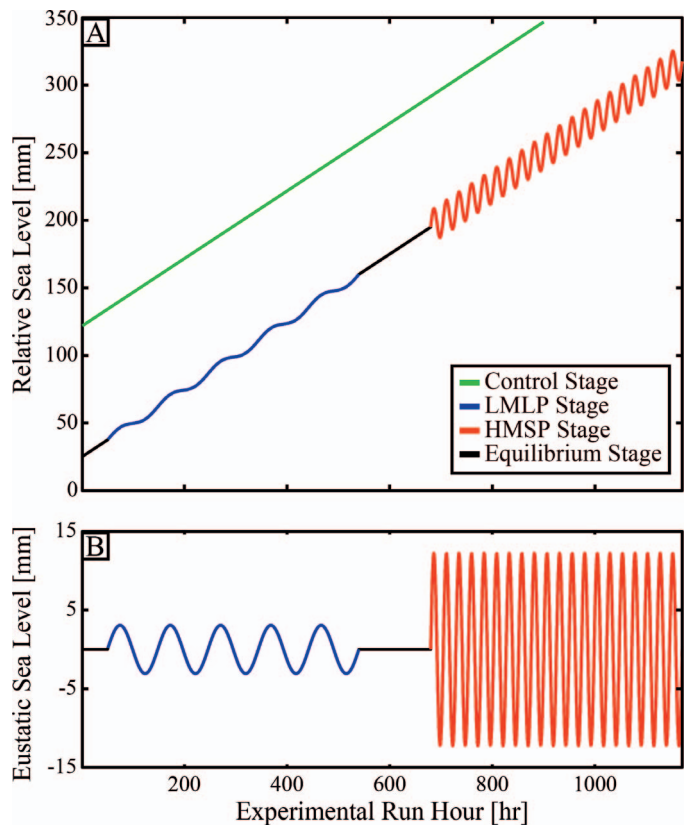


FIG. 2.—**A)** Relative-sea-level change over the course of the three experimental stages. **B)** History of sea level in each experimental stage after long-term trend has been removed; as such this is similar to eustasy for field-scale systems.

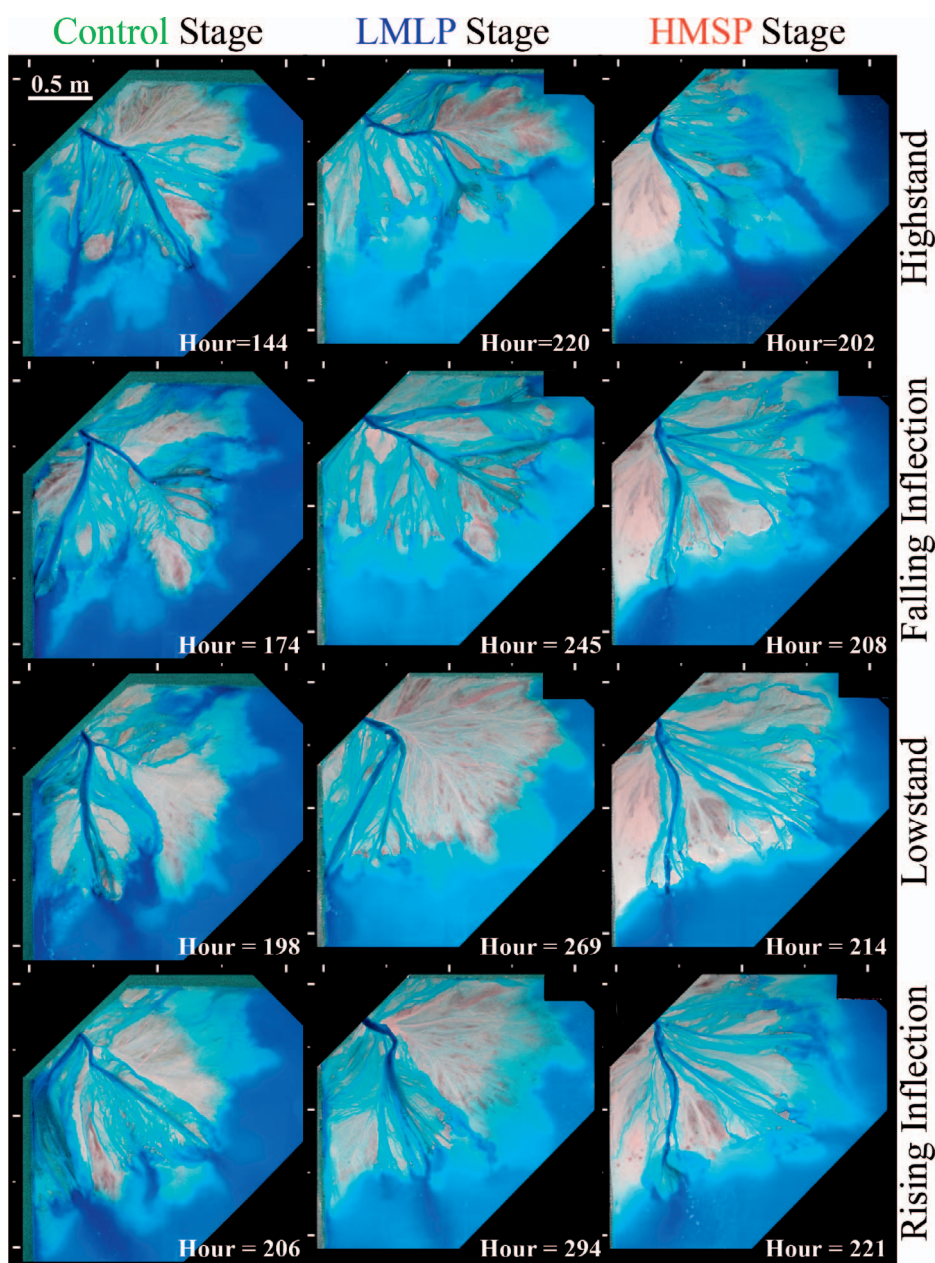


FIG. 3.—Overhead images of the three experimental stages. Images display system morphology at key points through a RSL cycle, or equivalent durations into a cycle of duration equal to  $T_c$  for the control stage.

stage. Li et al. (2016) showed that systems with values of  $H^* \gg 1$  and/or  $T^* \gg 1$  are associated with stratigraphic RSL signal storage. As such the first experimental stage will highlight storage due to RSL period and the second stage will highlight storage due to RSL magnitude. In each stage RSL cycled for 490 run-hours, producing approximately 120 mm of stratigraphy per stage. Experimental stages had slight differences in initial sea level. However, the duration of each stage was sufficient to generate tens of channel depths' worth of stratigraphy, thus reducing the importance of initial conditions on the trends discussed below.

Data were collected during the course of each experiment to define system morphodynamics and stratigraphy. Starting with system morphodynamics, a digital camera mounted directly above the basin collected photographs of the active delta top every 15 minutes. These images are used to analyze the evolving flow field of each experiment (Fig. 3).

A FARO Focus3D-S 120 laser scanner was used to monitor the topography in each experiment. This instrument captures an elevation

point cloud that can be converted into digital elevation models (DEMs) with horizontal grid spacing of 5 mm in the down-basin and cross-basin directions and with a vertical resolution less than 1 mm. DEMs cover an arc defined by a radius of 1.3 m from the entrance to the basin. Locations inboard of this arc were generally either delta top or upper delta foreset for most of the experiment (Fig. 1C). The laser scanner also houses a digital camera such that each point is tagged with an RGB color value. One scan was taken near the end of each run hour with the flow on, while a second scan was collected at the end of each run hour with the flow turned off. These color-coded digital elevation models can be used for both morphodynamic and stratigraphic analysis. The co-registered DEMs and digital images allow the flow field to be directly tied to topography, which aids morphodynamic analysis. For stratigraphic analysis, the topography can be used to construct synthetic stratigraphic volumes. This is done by stacking all topographic scans and clipping scans for erosion.

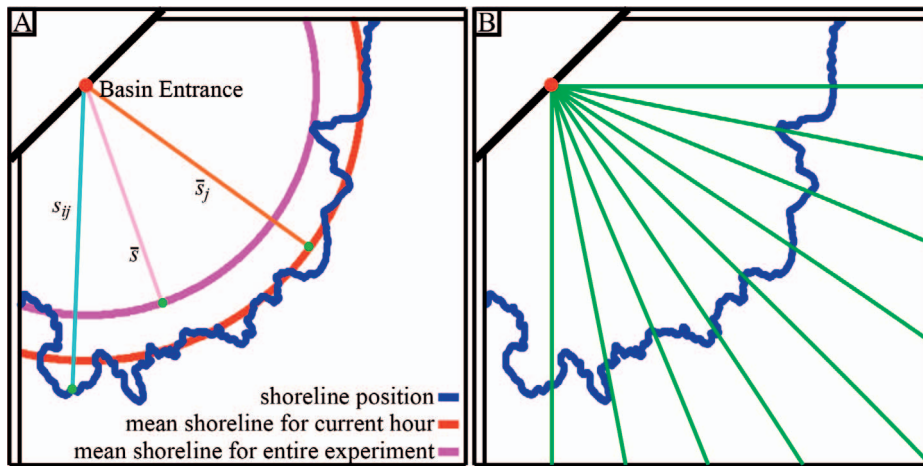


FIG. 4.—Definition sketch of key variables and parameters used in the shoreline analysis. **A)** Sketch detailing shoreline position, mean shoreline position for a given run hour, and mean shoreline position for an entire experiment. **B)** Sketch detailing location of transects used in calculation of shoreline migration rate and variability of this rate.

Finally, at the end of each experiment we sectioned the deltas along cross-sectional transects at 0.76 m and 1.22 m from the basin infeed point. These locations were approximately half-way down the delta top and the mean shoreline, respectively. This was done by inserting a metal wedge into the deposit after the sea level in the basin was raised to an elevation that flooded the entire deposit. The metal wedge was then filled with dry ice and methanol, which resulted in a chemical reaction that lowered the temperature of the wedge to a value sufficient to freeze the pore water in the deposit and the surrounding deposit to the wedge. The wedge was then extracted from the basin, providing a view of the preserved stratigraphy, which was then photographed with digital cameras. We define the structure of the strata observed in these images as the physical stratigraphy.

**RESULTS**

In this section we present results that characterize the influence of RSL cycle magnitude and period on deltaic morphodynamics and the resulting stratigraphy. We are particularly interested in comparing these morphodynamics and stratigraphic products to those produced in systems with constant forcings. As such, results from most analyses will include a comparison to our control experiment. We start by characterizing the morphodynamics in each experiment, focusing on those that are closely tied to depositional processes. We then characterize the stratigraphy of each experiment by use of stacked topographic scans clipped for erosion (synthetic stratigraphy) coupled to our limited number of physical-stratigraphy images.

*Morphodynamics*

**Shoreline Response to RSL Cycles.**—We are interested in how RSL cycles influence both the mean location and the rate of movement of the shoreline in addition to the variability of these parameters. Our interest in shoreline dynamics stems from the importance of this boundary in separating terrestrial and marine processes, and because transport systems tend to deposit sediment when reaching the shoreline. We quantify the mean shoreline location, the variability in this location relative to the basin entrance, and transgression and regression rates. Combined, these variables set depositional environments (marine vs. terrestrial) which are tied to stratigraphic architecture.

Using the DEMs and measured time series of sea level, we identify a line that defines the shoreline each run hour. The distance from the basin entrance to the shoreline,  $s_{ij}$ , was then calculated for all points that define this line, where  $i$  is an index that refers to each spatial measurement of distance to the shoreline and  $j$  is an index that refers to the run hour (Fig. 4A). We use these measurements of  $s_{ij}$  to calculate the mean distance to the

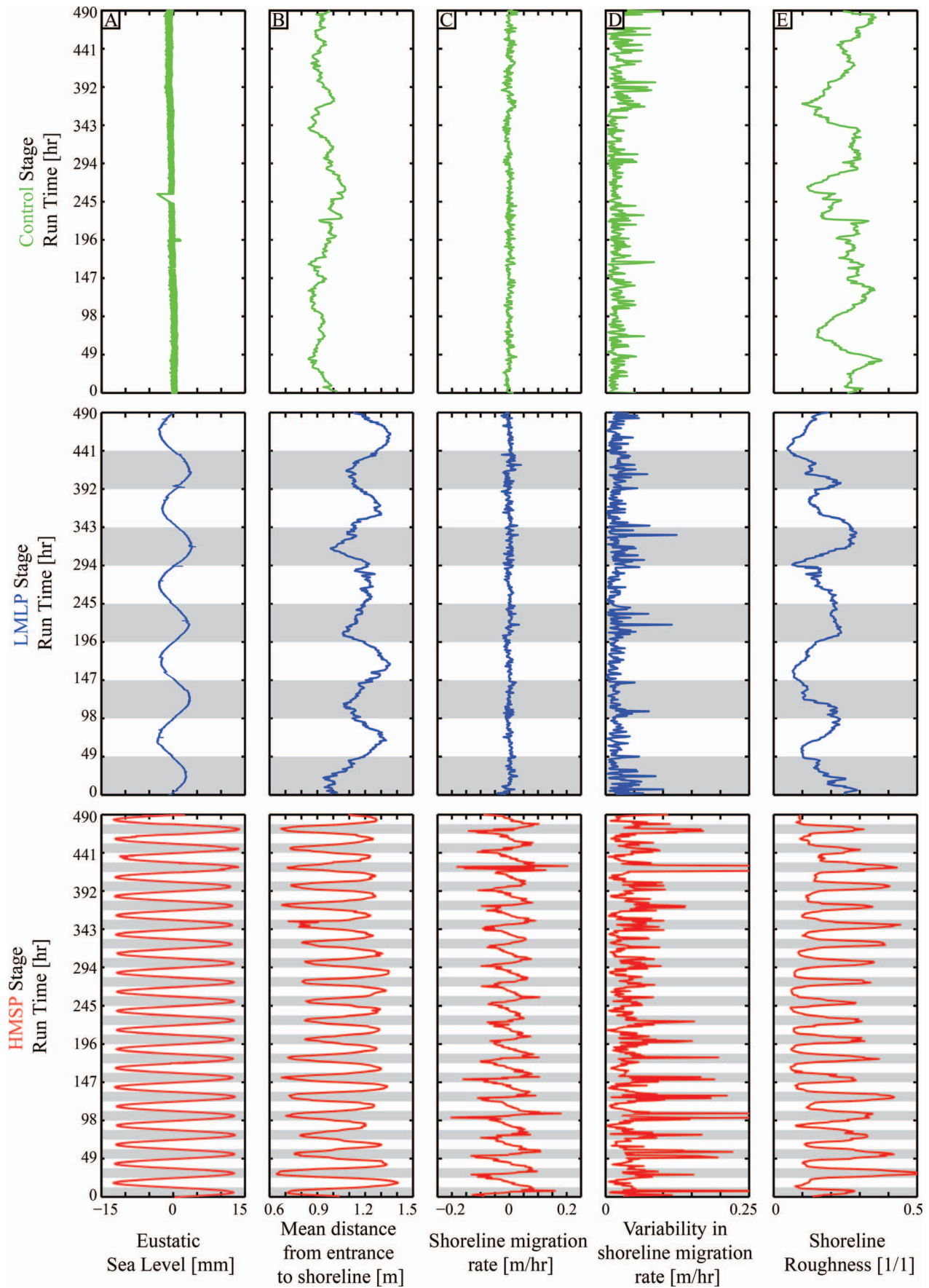
shoreline for each run hour ( $\bar{s}_j$ ) and the mean distance to the shoreline for an entire stage ( $\bar{s}_{St}$ ), where again stage refers to a portion of an experiment where sea level is fluctuating with a constant magnitude and period. Starting with the control experiment, we observe differences in  $\bar{s}_j$  relative to  $\bar{s}_{St}$  with magnitudes up to 0.14 m (Fig. 5B). Transgressions and regressions of the shoreline in the control experiment are the result of autogenic sediment storage and release events, associated mainly with delta lobe avulsions. As expected, in both the LMLP and HMSP stages the position of  $\bar{s}_j$  is tied to eustatic sea level, with high eustatic sea level corresponding to short  $\bar{s}_j$  and vice versa. The amplitude of changes to  $\bar{s}_j$  in the stages with RSL cycles are larger than autogenic changes observed in the control experiment. Next, we characterize the mean response of  $\bar{s}_j$  to one full cycle of RSL through ensemble averaging, where the averaging is done for records of duration equivalent to one  $T_{RSL}$ . As such, we are averaging the response to five cycles in the LMLP stage and 20 cycles in the HMSP stage (Fig. 6). To generate a similar plot for the control experiment, we ensemble average sequential segments of the control experiment that have duration equal to one  $T_c$ , starting from the beginning of the control stage. While both stages with RSL cycles show a response of  $\bar{s}_j$ , with maximum transgression at the peak of a sea-level cycle, the magnitude of this response was two times greater in the HMSP stage than in the LMLP stage.

Motivated by an analysis of shoreline movement in the earlier-discussed XES experiments (Kim et al. 2006), we are interested in defining the influence of RSL cycles on the rate of shoreline movement and the variability in this rate. To do this we track the position of the shoreline each run hour along nine transects each of which originate at the basin entrance and are separated by an angle of  $\pi/8$  (Fig. 4B). We then calculate the rate of shoreline movement along each transect for sequential run hours. This allows us to calculate the mean rate of shoreline movement during a given run hour ( $\dot{s}_j$ ) (Fig. 5C) and the standard deviation of this rate  $\sigma(\dot{s}_j)$  (Fig. 5D). Similarly to our analysis of  $\bar{s}_j$  we ensemble average all cycles for a given stage to see the response of  $\dot{s}_j$  and  $\sigma(\dot{s}_j)$  to an average RSL cycle (Fig. 6C, D). We observe a clear response of  $\dot{s}_j$  and  $\sigma(\dot{s}_j)$  to RSL cycles in the HMSP stage with  $\dot{s}_j$  approximately one-quarter out of phase with RSL and  $\sigma(\dot{s}_j)$  being in phase with RSL cycles. Observations for the LMLP stage are less clear. A muted signal of  $\dot{s}_j$  is observed while  $\sigma(\dot{s}_j)$  shows no response above the autogenic perturbations.

Our next morphodynamic analysis is focused on the roughness of the shoreline ( $R_S$ ). We define  $R_S$  as

$$R_S = \sqrt{\frac{1}{N} \sum_{i=1}^N \left( \frac{s_{ij} - \bar{s}_j}{\bar{s}_j} \right)^2} \tag{4}$$

where  $N$  is the total number of measurements that define the shoreline at



run hour  $j$  (Figs. 5E, 6E). In both the HMSP and LMLP stages we observe changes in  $R_S$  that are in phase with RSL. However, the response of  $R_S$  to RSL is much stronger in the HMSP stage than in the LMLP stage.

We note that all metrics used to define the shoreline and its movement show stronger responses in the HMSP stage than in the LMLP stage. In fact, some of the metrics ( $\dot{s}_j$  and  $R_S$ ) show barely detectable signals in the LMLP stage while no detectable signal is found for  $\sigma(\dot{s}_j)$ . Interpretation of these trends will be discussed further in later sections.

### Flow Confinement

Next, we characterize the influence of RSL cycles on the fraction of the terrestrial deltaic surface covered by active flow. This is motivated by interpretations of paleo-system configurations made from outcrop observations (Van Wagoner et al. 1990; Catuneanu et al. 2009) and results from physical (Heller et al. 2001) and numerical (Karssenberg and Bridge 2008) experiments. These studies suggest that the fraction of the terrestrial surface covered by flow should decrease as flow is confined in incised channels during base-level fall, and that this fraction should rise as confinement is lost during base-level rise. Observations of the active deltaic surface suggest that changes in flow confinement are linked to position within a RSL cycle (Fig. 3). To measure this in our experiments we start by using the topographic maps and imposed time series of sea level to extract all terrestrial delta pixels (elevation > sea level). Each terrestrial delta cell is converted to an area equal to  $2.5 \times 10^{-5} \text{ m}^2$ , determined by the geometry of the imposed topographic grid. This allows the total terrestrial area,  $A_{TD}$ , to be calculated for each run hour. Next, we calculate the area of the terrestrial delta covered by flow,  $A_{wet}$ . Using the red ( $R$ ), green ( $G$ ), and blue ( $B$ ) color bands recorded in the digital images collected by the scanner, we calculate the color intensity,  $I$ , of the terrestrial cells as

$$I = \frac{B - G - R}{B + G + R} \quad (5a)$$

when the flow was dyed blue and as

$$I = \frac{R - G - B}{B + G + R} \quad (5b)$$

when the flow was dyed red. A threshold intensity value is then set to separate wet from dry regions. This threshold was picked by identifying a value that on visual inspection appeared to accurately separate the two regions. Finally, the wetted fraction ( $f_w$ ) of the terrestrial delta is calculated as

$$f_w = \frac{A_{wet}}{A_{TD}} \quad (6)$$

Similar to attributes defining the morphodynamics of the shoreline in response to RSL cycles, we calculate an ensemble average response of  $f_w$  to one full cycle of RSL (Fig. 7).

In the LMLP and HMSP stages a similar response of  $f_w$  is observed. This response includes a maximum in  $f_w$  during RSL highstand and minimum during RSL lowstand, consistent with existing theory (Posamentier and Vail 1988; Van Wagoner et al. 1990; Catuneanu et al. 2009). However, the magnitude of the response, relative to the control experiment, is greater in the HMSP relative to LMLP stage. A similar calculation for the ensemble averaged  $f_w$  over a period equivalent to  $T_c$  in the control experiment shows no significant structure. The response of  $f_w$  for the stages

with RSL cycles is in phase with RSL, and we note that by analysis of Equation 6 this response could occur by simply reducing  $A_{TD}$  through transgression during RSL rise with a constant proximal to distal increase in confinement. However, we almost always observed a proximal to distal decrease in flow confinement associated with distributary-channel networks.

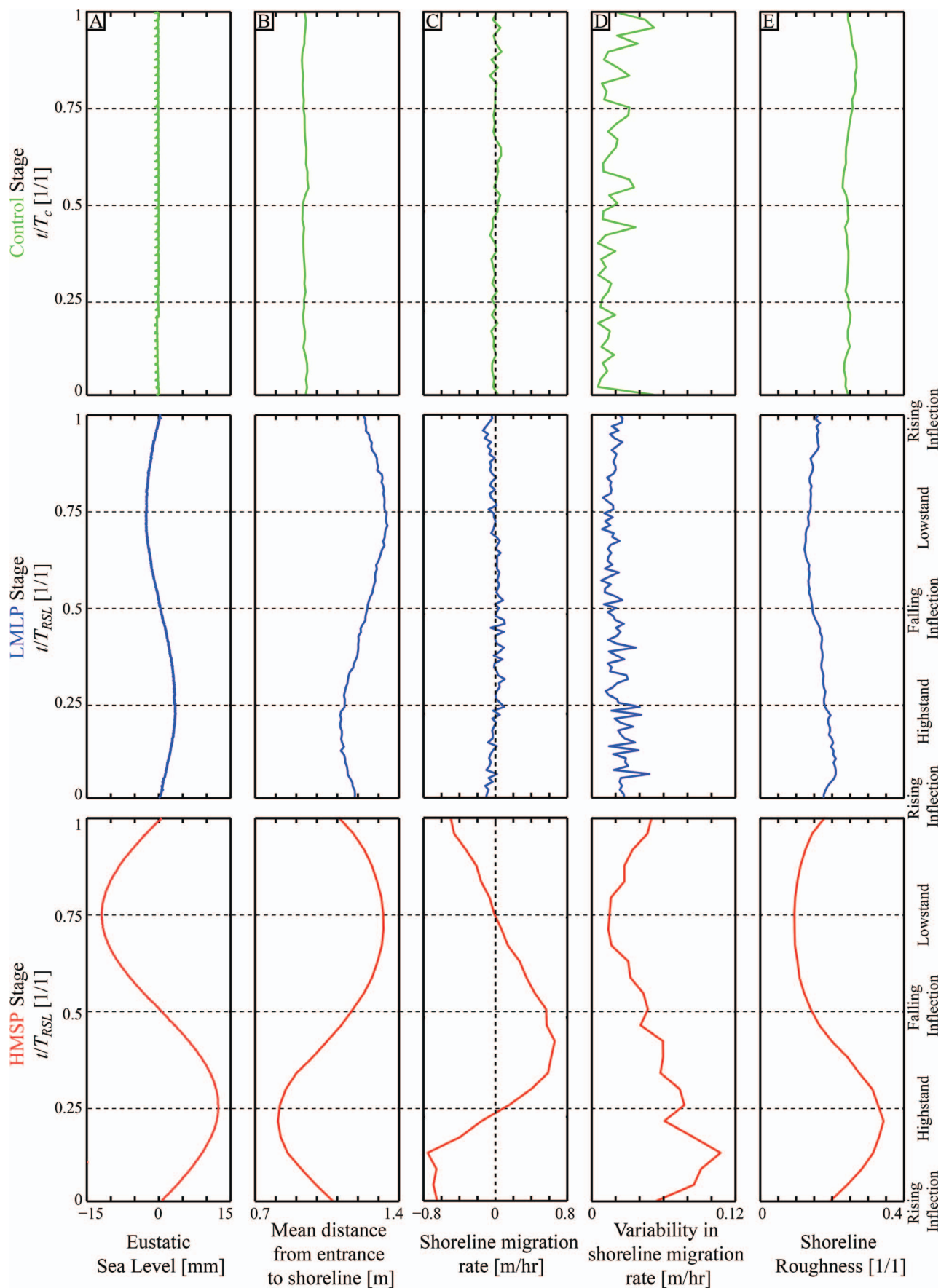
### System Mobility

Several studies suggest that the mobility of deltaic systems, here defined as the movement of a sediment transport system through slow lateral migration and/or punctuated avulsion, is minimized during the troughs of RSL cycles and maximized during the crest of RSL cycles (Van Wagoner et al. 1990; Heller et al. 2001; Karssenberg and Bridge 2008). Similar to  $f_w$ , the tie between RSL and system mobility is linked to the lateral confinement of flow in valleys during falling RSL and valley filling with associated high avulsion rates during rising and high RSL. Because paleo-valley fills and channel avulsion deposits are prominent stratigraphic features in deltaic stratigraphy, we are interested in evaluating the processes necessary to generate them. Previous experimental studies characterized system mobility by quantifying the amount of time necessary for 95% of a delta top to be visited by flow in overhead images of the transport system (Cazanaceli et al. 2002; Kim et al. 2010; Straub and Esposito 2013). Given the high temporal resolution of our topographic data, we decide to take a different approach and measure a proxy of mobility by tracking the number of grid locations that experience measurable geomorphic work over the course of a run hour.

We refer to elevation changes, either erosion or deposition, as modifying the transport surface and as such define modification in our experiments as a change in elevation of at least 1 mm, the vertical resolution of our DEMs. We track surface modification along strike-oriented transects (given the geometry of our basin these are semicircles) defined by specified radii measured from the basin entrance. As such, these transects are roughly oriented perpendicular to the mean flow direction (Fig. 8A). This is done for transects ranging from 0.35 m to either 1.2 m (the control stage) or 1.3 m (stages with RSL cycles) from the basin entrance, each separated by 0.05 m. For each transect and each run hour, we measure the fraction of grid cells along a transect that experience surface modification,  $f_m$ . We ensemble average the  $f_m$  response to an RSL cycle by calculating  $f_m$  for each run hour and for each transect, and then averaging all measurements that share the same distance from the basin entrance and the same number of run hours into a RSL cycle. This produces time-space maps of  $f_m$ , where time is presented as the fraction of time into a full cycle of RSL and distance is relative to the basin entrance (Fig. 8B–D). On each time-space map we also plot a line that represents the mean shoreline location, to aid interpretation of trends.

From the time-space maps of surface modification we make the following observations: 1) The control stage shows the lowest fraction of surface modification of all of the stages and no consistent temporal trend over the course of a  $T_c$  cycle. 2) At most time-space pairs, the LMLP stage shows a slightly higher fraction of surface modification, compared to the control experiment. The reworking shows only muted spatial and temporal trends, with modification minimized during periods of low RSL. 3) The HMSP stage shows clear spatial and temporal trends in modification compared with the other two stages;  $f_m$  values calculated at the mean shoreline and just beyond are far in excess of those observed in the two other stages. During periods of low RSL,  $f_m$  values upstream of the mean

FIG. 5.—Data defining the measured response of shorelines to changes in RSL and the variability of this response. **A)** Time series of measured eustasy in each experimental stage. **B)** Time series of the mean distance from the basin entrance to the shoreline. **C)** Time series of the mean shoreline migration rate. Negative values indicate shoreline moving landward. **D)** Time series of the variability of the rate of shoreline migration. **E)** Time series of the shoreline roughness. Gray bars indicate periods when sea level was higher than average.



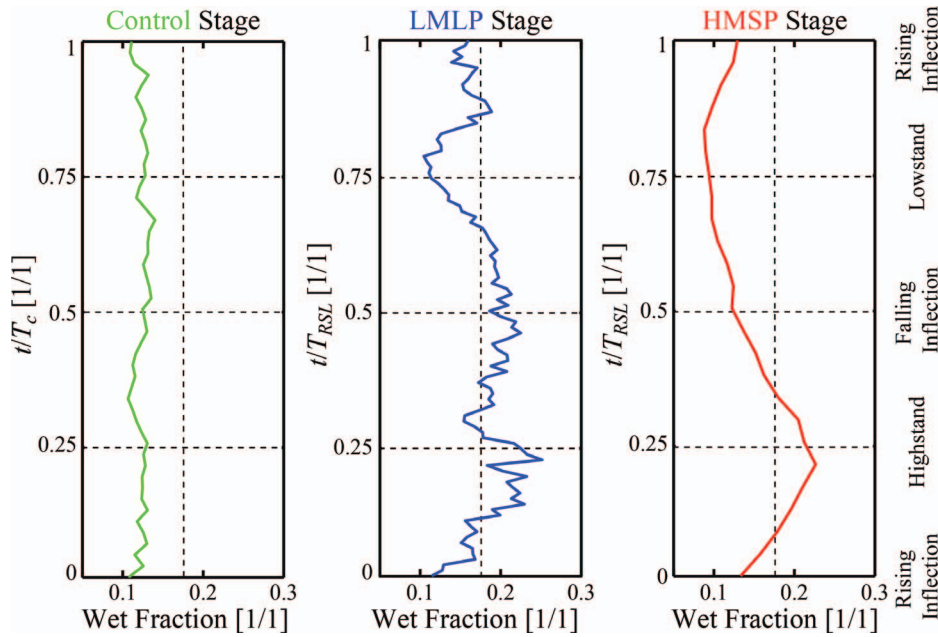


FIG. 7.—Data defining ensemble average response of the wetted fraction of the terrestrial delta top to changes in RSL.

shoreline are also extremely low, suggesting low system mobility. During rising eustatic sea level, locations upstream of the mean shoreline show  $f_m$  values higher than those measured at most locations in the control and LMLP stages.

**Stratigraphy**

In the following section we characterize the influence of RSL-cycle magnitude and period on resulting strata. Similarly to our morphodynamic characterization, we compare the temporal and spatial scales of stratigraphic products in stages that experienced RSL cycles to both the mean and stochastic attributes of the stratigraphy from our control experiment.

**Mass Extraction**

Our first stratigraphic analysis centers on the influence of RSL cycles for the storage of sediment in terrestrial and marine settings. The motivation is similar to the analysis of Li et al. (2016), who worked with this same set of experiments. In their study, Li et al. calculated the average deposition rate along strike-oriented transects, for each hour of the three experimental stages. This was done at relatively proximal and distal locations on the experimental delta tops. They found that when either RSL-cycle magnitude or period exceeded the spatial or temporal scales of autogenic processes, the period of the RSL cycle could be found in the power spectra of deposition rates.

Whereas Li et al. focused on analysis of mean deposition rates along individual strike transects, our aim is to analyze the volumetric extraction of mass in settings that are dominantly terrestrial vs. dominantly marine. We start this analysis by generating a time series of the total volume of sediment stored inboard of the mean shoreline of both the control experiment and the experiment with RSL cycles,  $V_{inboard \bar{s}}$  (Fig. 9B). We focus on this region because we expect enhanced volumetric growth during periods of high eustatic sea level as channels meet a shoreline inboard of

its mean position. Coincidentally, the position of the mean shoreline in each stage occurred at a distance where approximately 48–51% of the mass input to the basin was extracted to deposition. As such, approximately half of the sediment was deposited in dominantly terrestrial settings and half in dominantly marine settings.

In each experimental stage a long-term growth of  $V_{inboard \bar{s}}$  is observed, resulting from the long-term generation of accommodation in the basin. We subtract this long-term trend, estimated with a least-squares linear regression of the growth of  $V_{inboard \bar{s}}$ , to analyze the influence of sea-level cycles in perturbations of  $V_{inboard \bar{s}}$  (Fig. 9C). Finally, similarly to our analysis of morphodynamic attributes, we generate an ensemble average of the response of the detrended  $V_{inboard \bar{s}}$  to a cycle of RSL (Fig. 9D). In both the LMLP and HMSP stages we see a clear response of the detrended  $V_{inboard \bar{s}}$  to RSL cycles in the ensemble average, with a phase shift of one quarter cycle and a response that is of similar magnitude in both stages with sea-level cycles.

**Stratigraphic Architecture**

While the volumetrics discussed above inform us about long-term trends in mass extraction, we are also interested in the architecture of the stratigraphy resulting from each experiment, including the geometry and grain sizes of sequences. We start our characterization of stratigraphic architecture with panels of physical stratigraphy imaged along proximal and distal strike transects (Fig. 10). In our control experiment we observe strata composed of coarse channel-fill deposits and fine-grained overbank deposits at the proximal transect. Prominent channel–levee deposits segregate the coarse channel-body deposits from the fine overbank. The stratigraphy from the proximal transect of the experiment with RSL cycles also contains coarse channel-fill deposits and fine overbank zones but lacks the well-developed levees found in the strata of the control experiment. While the stratigraphy of the LMLP and control stages share similar numbers of channel bodies, the strata of the HMSP stage contain slightly

FIG. 6.—Data defining the ensemble average response of shorelines to changes in a cycle of RSL and the variability of this response. **A)** Measured eustasy in each experimental stage. **B)** Distance from the basin entrance to the shoreline as a function of run time. **C)** Response of the mean shoreline migration rate. Negative values indicate shoreline moving landward. **D)** Response of the variability of the rate of shoreline migration. **E)** Response of the shoreline roughness.

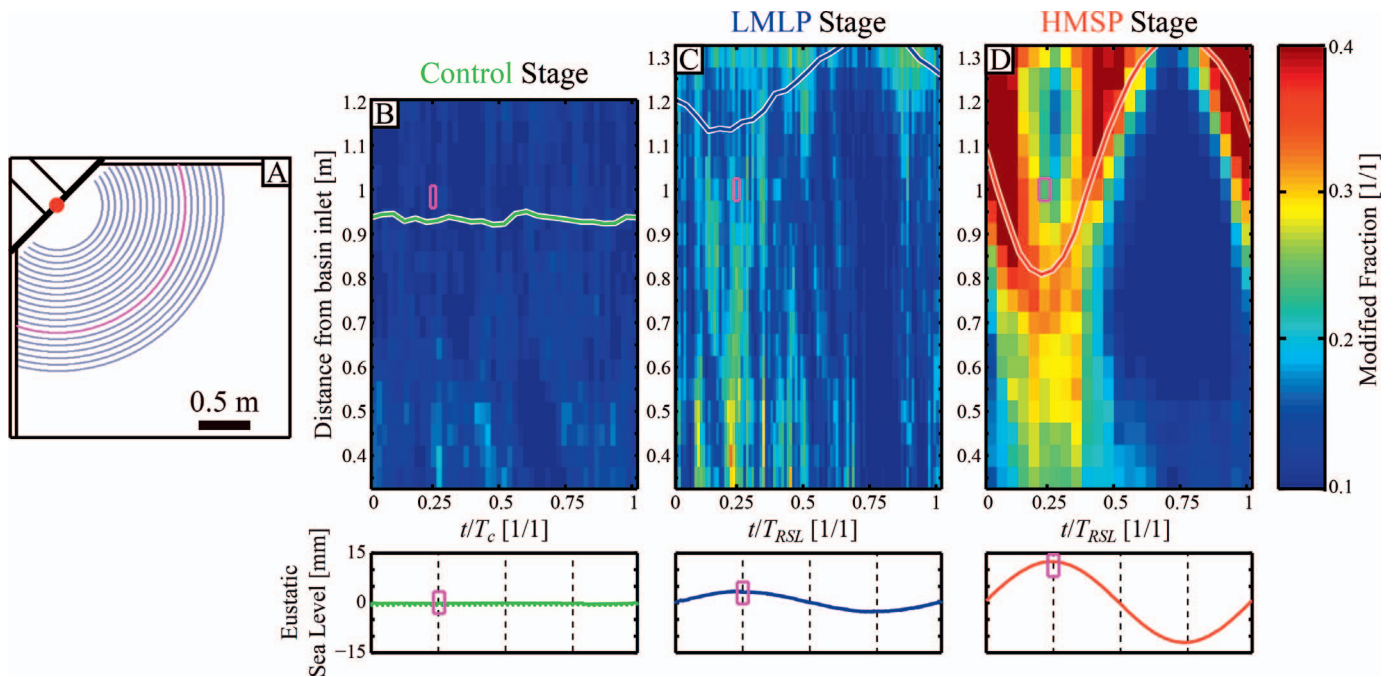


FIG. 8.—Data defining how the average fraction of a geomorphic surface modified by erosion or deposition over the course of a run hour varies from proximal to distal basin locations and as a function of temporal position into a RSL cycle. **A)** Schematic of delta basin illustrating location of 20 transects used in analysis of surface modification fraction. **B–D)** Time–space maps of surface modification fraction for the control, LMLP, and HMSP stages, respectively. Below each time–space map a plot of measured eustatic sea level is provided for reference. Solid lines within each time–space map indicate the ensemble average location of the shoreline. Magenta-highlighted transect in basin schematic, outlined time–space map cells, and highlighted eustatic sea level at one quarter way into RSL cycle illustrate how cells in the time–space maps are linked to distance from basin inlet, time into a RSL cycle, and associated value of eustatic sea level.

more channel bodies, with more frequent evidence of incision at their bases.

The stratigraphy of the distal strike transects are dominantly composed of coarse terminal-channel-lobe deposits and fine overbank and marine strata (Fig. 10D–F). The distal stratigraphy of the control experiment is markedly coarser than the strata of the stages with RSL cycles, with each coarse lobe deposit separated by thin fine-grained strata that are relatively laterally continuous. In contrast the average size of lobe deposits is less in the LMLP stage, relative to the control strata, and further less in the strata of the HMSP stage. These differences in lobe sizes are associated with an increase in the volume of fine strata as the magnitude of RSL cycles increased from the control stage to the LMLP and finally to the HMSP stage.

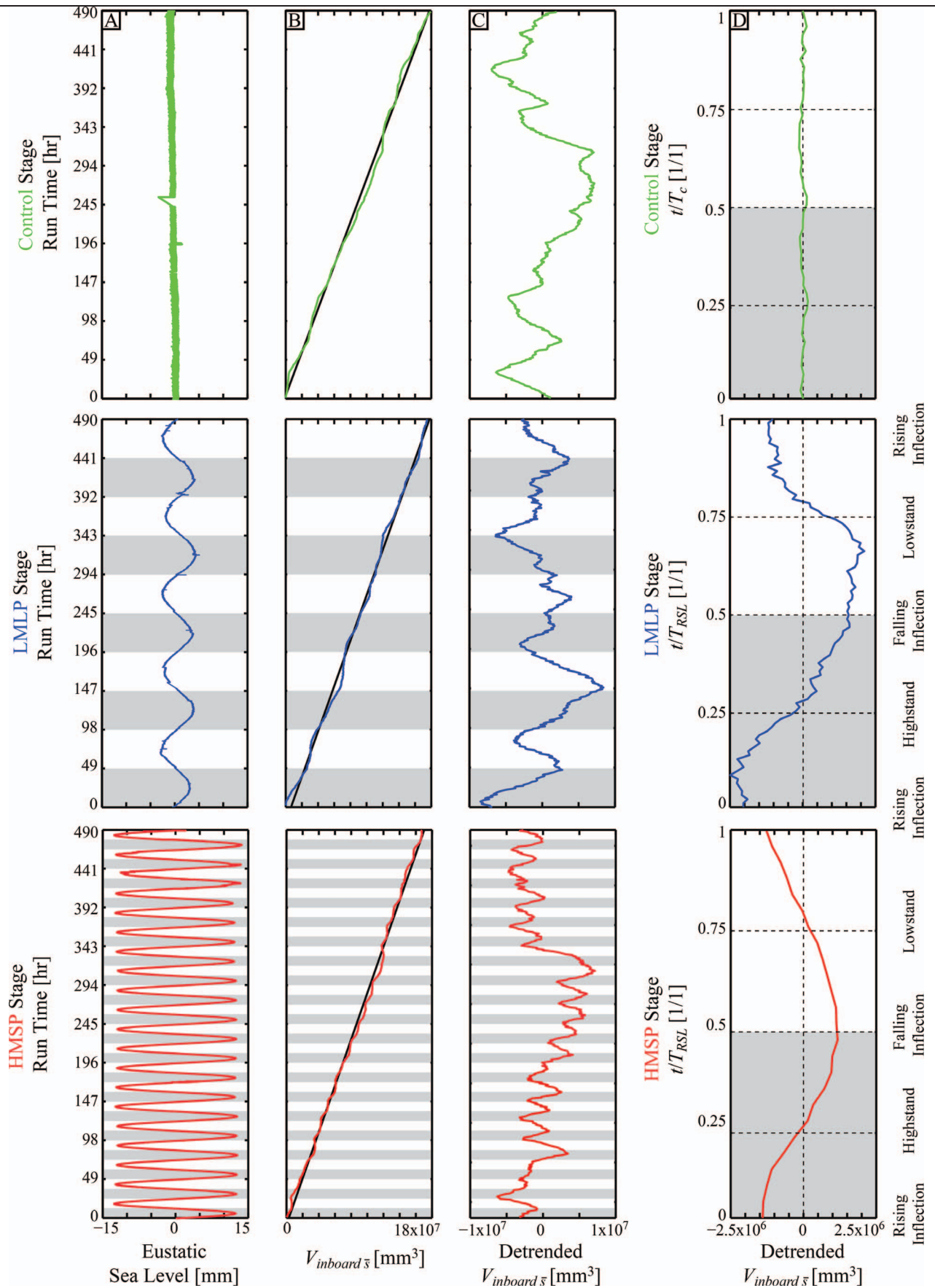
We quantify the differences in content of coarse sand in the strata of each stage at the proximal and distal transects by taking advantage of the commercially dyed coarse sediment and the dominantly white fine sediment. Similarly to our analysis of the wetted terrestrial delta-top fraction, we use the R, G, and B color bands of the physical-stratigraphy images to calculate the color intensity of each pixel using Equation 5 and utilize a threshold intensity value that through visual inspection appears to separate coarse from fine sediment. We then calculate the fraction of coarse colored sediment for the stratigraphy of each stage at each transect (Fig. 11). This allows us to make the following observations. For both the proximal and distal transects the stratigraphy of the HMSP stage has less coarse colored sediment than the strata of the LMLP and control stages. At

the proximal transect the strata of the control and LMLP stages share similar colored sand fractions, while the control strata of the distal transect has markedly more coarse colored sediment than the LMLP stage strata. For each stage the strata have more coarse colored sediment at the distal compared to the proximal transect.

While the physical stratigraphy gives valuable information on the segregation of particles based on grain size, unfortunately we were able to collect only two strike sections per stage. In addition, while the architecture of the physical stratigraphy is influenced by RSL cycles, defining environments and timing of deposition relative to these cycles based solely on the physical stratigraphy would require imprecise interpretations. To overcome these problems, we assemble volumes of synthetic stratigraphy, generated by stacking DEMs with topography clipped to account for sediment removed during erosional events (Martin et al. 2009). Knowledge of the run time and sea level associated with each DEM allows us to paint this synthetic stratigraphy with attributes like depositional environment (terrestrial vs. marine) and the timing within a RSL cycle when sediment at a particular location was deposited.

Using the co-registered sea level and DEMs, we separate portions of the stratigraphy deposited in terrestrial vs. marine settings. We use our knowledge of topographic evolution and sea-level history to define parasequences, rather than relying on outcrop observations, which is the common practice. Here we define parasequences as genetically related beds deposited in terrestrial conditions bounded by sediment deposited in marine settings and their correlative surfaces. In practice, given our limited

FIG. 9.—Data defining the measured response of deposit volume inboard of the ensemble average shoreline to changes in RSL. **A)** Time series of measured eustatic sea level in each experimental stage. **B)** Time series of the growth of the deposit volume inboard of the mean shoreline for each hour. Solid black line represents long-term trend. **C)** Time series of the detrended deposit volume inboard of the mean shoreline. Gray bars indicate periods when sea level was higher than average. **D)** Ensemble average of the measured detrended deposit volume inboard of the mean shoreline from each RSL cycle.



experimental data coverage in deep marine settings, we focus on the terrestrially deposited beds and their bounding marine deposits. When viewed in dip panels, we note prominent parasequences in the stratigraphy of the control stage that resulted from autogenic transgressions and regressions of the shoreline in conjunction with active deposition (Fig. 12A). The constituent layers of the strata that define these parasequences extend laterally up to 0.75 m before pinching out, and thicknesses are up to 13 mm. The parasequences in the LMLP and HMSP experiments show differences with the control experiment. These include preservation of beds deposited in marine settings that extend upstream of those found in the control experiment (Fig. 12 and additional dip sections not shown here, which can be constructed using data stored in online repository). In addition, the thickness of the parasequences in the LMLP stage (Fig. 12B) exceeded those of the control stage, while parasequence thickness in the HMSP stage (Fig. 12C) never reached the thicknesses seen in the control stage.

Next, we paint the synthetic stratigraphy by the position within a RSL cycle in which sediment was deposited (Fig. 13). We do this to test if the RSL cycles control the spatial and temporal distribution of strata in basin-margin clinoforms. Here we compare stratigraphy in both dip (Fig. 13A, B) and strike sections from relatively proximal (Fig. 13C, E) to relatively distal (Fig. 13D, F) locations.

Starting with the stratigraphy viewed in dip section, we observe no dominant spatial trend in the timing of deposition within a cycle of RSL in the LMLP stage. There is, however, a strong spatial trend in the HMSP stage dip stratigraphy. While stratigraphy from the basin entrance to approximately 0.7 m from the source shows no clear preference for position within a RSL cycle, from 0.7 to 1.2 m from the source deposition occurred dominantly during RSL highstands. Downstream of this zone deposition occurs dominantly during RSL lowstands. In strike transects we observe trends similar to those seen in dip, with strata in the proximal transects of the HMSP stage constructed mainly of highstand deposition and distal strata constructed mainly of lowstand deposition.

The spatial trends in timing of deposition during a RSL cycle, noted above, have significance for ongoing discussions surrounding sequence stratigraphic models. Early models in this field hypothesized that deltaic topsets were constructed exclusively during rising and high sea level and that falling and low sea level resulted in sediment bypass of the topset to more distal settings (Posamentier and Vail 1988; Van Wagoner et al. 1990). More recently, several authors have used field observations and numerical and physical experiments to suggest that deltaic topset deposition can occur during all phases of a RSL cycle (Schumm 1993; Swenson and Muto 2007; Burgess and Prince 2015; Nijhuis et al. 2015). To address this question in our experiments, we start by quantifying the thickness of strata preserved in each deposit as a function of both the distance from the basin entrance and the time into a RSL cycle. For cross sections positioned every 0.1 m from the basin entrance, we calculate how a normalized deposit thickness,  $D^*$ , varies according to position in a sea-level cycle (or cycle of duration  $T_c$  for the control experiment, as in earlier analysis).  $D^*$  is defined as

$$D^* = \frac{\bar{D}(x, t/T_{RSL})}{\sigma} \quad (7)$$

where  $\bar{D}(x, t/T_{RSL})$  is the mean thickness of strata deposited in one hour, positioned a distance  $x$  from the basin entrance, and during a time,  $t/T_{RSL}$ , into a RSL cycle. This deposit thickness is then normalized by the pseudo-subsidence generated in one run hour,  $\sigma$ . A  $D^*$  value equal to 1 thus represents an average thickness of strata deposited in one hour, at a given time into a RSL cycle, that equals the amount of accommodation generated by pseudo-subsidence during that hour. We then generate an ensemble average response to an RSL cycle for each stage at each analyzed distance from the basin entrance (Fig. 14).

While some variability exists in the time–space maps of  $D^*$  for the control experiment, most values are close to 1.  $D^*$  values in the LMLP time–space maps show strong variability, which lacks much structure in time or space. Values of  $D^*$  greater than 1 are more commonly found inboard of the mean shoreline during sea-level highstands, and conversely values less than 1 are more commonly found inboard of the mean shoreline during lowstands. Clear structure is found in the  $D^*$  time–space maps from the HMSP stage. Thick deposits are constructed near the shoreline over the course of the entire sea-level cycle. Inboard of the mean shoreline, thick deposits are preferentially constructed during highstands and vice versa for lowstands.

We use the data presented in Figure 14 to calculate the fraction of strata deposited during highstands,  $F_{HS}$ , as a function of distance from the basin inlet. By highstand we simply mean that eustatic sea level was higher than 0. In both the HMSP and LMLP stages  $F_{HS}$  is greater than 50% in regions inboard of the mean shoreline, indicating preferential deposition during conditions of high eustatic sea level (Fig. 15A). The LMLP-stage strata show relatively constant  $F_{HS}$  fractions over the delta topset at  $\sim 0.65$ , while the HMSP-stage strata display a peak in  $F_{HS}$  located approximately halfway between the basin entrance and the mean shoreline, where  $F_{HS}$  equals 0.82. As such, the minimum fraction of topset deposition constructed during lowstand, equal to  $1 - F_{HS}$ , is 0.18.

While the  $F_{HS}$  plots indicate significant topset deposition during both highstands and lowstands, this metric does not quantify when during a sea-level cycle most deposition occurs, outside eustatic sea level being higher than the mean eustatic sea level. To quantify when, on average, deposition occurs in each experimental stage, we calculating a metric,  $\alpha_D$ , equal to

$$\alpha_D = \frac{1}{N} \sum_{i=1}^N \left( \frac{\bar{D}_i(x)}{\sigma} \frac{\eta_{ESL,i}}{M_{RSL}/2} \right) \quad (8)$$

where  $\bar{D}_i(x)$  is the mean thickness of strata deposited during run hour  $i$  at a distance  $x$  from the basin entrance,  $\eta_{ESL,i}$  is the eustatic sea level during run hour  $i$ , and  $N$  is the total number of run hours analyzed. For a given RSL cycle,  $\alpha_D$  theoretically could take any value between  $-1$  and  $1$ . A value of  $-1$  would represent a deposit constructed only when sea level was at the trough of a cycle, while a value of  $1$  would represent deposits constructed only when sea level was at the peak of a cycle. Analysis of  $\alpha_D$  curves as a function of distance from basin inlet (Fig. 15B) show that the topset of the LMLP stage was on average constructed with eustatic sea level just slightly higher than the mean of a cycle, with  $\alpha_D$  approximately equal to  $0.17 \pm 0.03$ , regardless of spatial position on the topset. More structure was observed in the plot of  $\alpha_D$  as a function of distance from basin inlet for the HMSP-stage deposit. Starting at 0.3 m from the basin inlet,  $\alpha_D$  increases from a value of 0.2 to a value of 0.45 at a distance of 0.8 m from the basin inlet and then decreases for more distal locations. Combined, the plots presented in Figure 15 suggest significant deposition over the entire course of sea-level cycles.

### Stratigraphic Completeness

Our final analysis centers on the temporal completeness of the strata preserved in each experimental stage. Stratigraphic records contain significant gaps over a range of time and space scales resulting from stasis on geomorphic surfaces and erosional events that remove previously deposited sediment. These gaps influence the temporal resolution of proxy environmental records stored in stratigraphy. Previous studies have used an array of stochastic and deterministic models to quantify the controls on completeness, but little data exist to test these models. For example, Sadler and Strauss (1990) examined the completeness of random-walk models with superimposed cyclical generation of accommodation, motivated by RSL cycles. Here we quantify how the magnitude and period of RSL cycles influences stratigraphic completeness in our experiments. Similarly

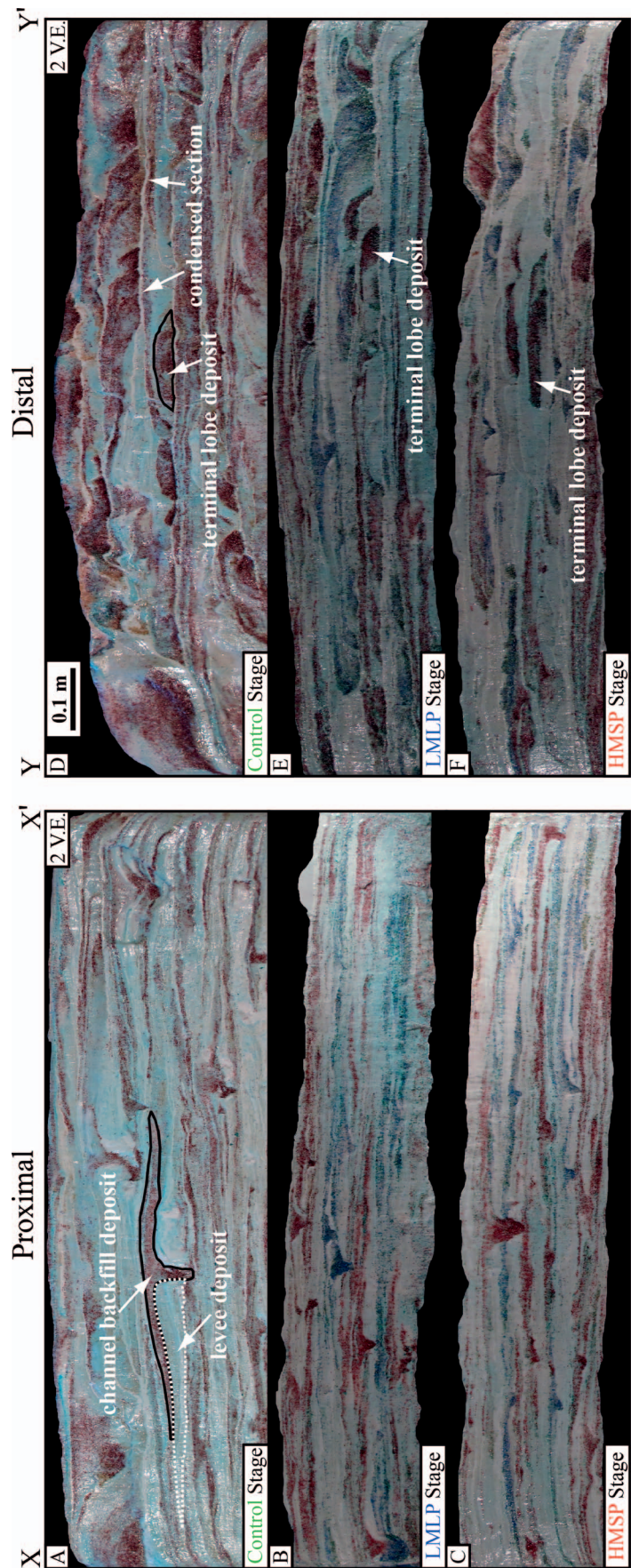


Fig. 10.—Images of preserved physical stratigraphy of the three experimental stages from A–C) proximal and D–F) distal strike-oriented transects. Panels are oriented as if one were looking downstream and displayed with a vertical exaggeration of 2. Location of transects are shown in Figure 1B.

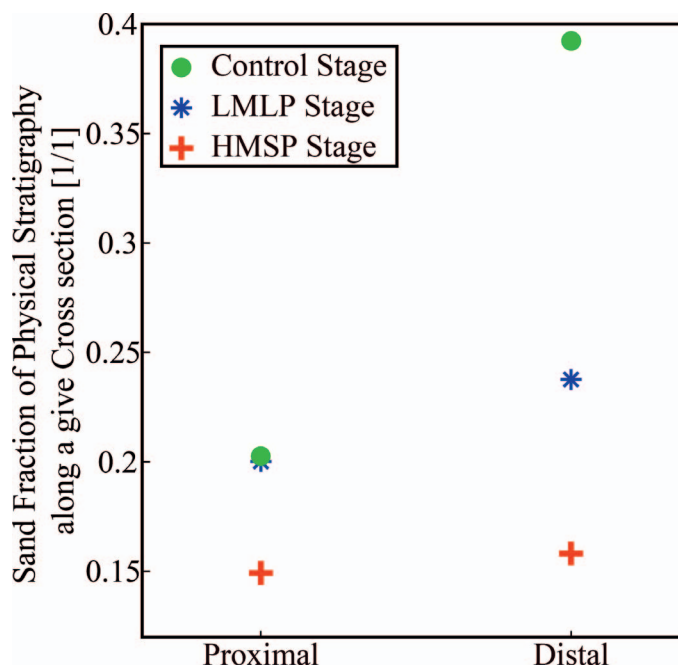


FIG. 11.—Colored sand as a fraction of total stratigraphic section measured from images of physical stratigraphy presented in Figure 10.

to previous studies (Sadler and Strauss 1990; Straub and Esposito 2013), we define stratigraphic completeness as the number of intervals,  $n$ , along vertical 1-D stratigraphic sections discretized at  $t$ , which leave a record in the form of any preserved sediment over the length of a given section that has a total time,  $T$ :

$$C = \frac{nt}{T} \quad (9)$$

We are interested in the completeness of each stage as it helps define if stratigraphic sections have sufficient temporal coverage to extract the sequencing of paleo-surface processes and environmental forcings. We also focus on completeness of entire experimental stages, as this provides adequate experimental run time to sample the full array of dynamics and products of each stage, rather than focusing for example on the completeness during one particular lowstand. As noted by Ager (1973) and quantified by Sadler and Strauss (1990) and Straub and Esposito (2013), stratigraphic completeness increases as  $t$  increases. Gaps in the stratigraphic record of systems with constant forcings occur due to periods of stasis on geomorphic surfaces and erosional events that occur due to stochastic autogenic channel dynamics. Processes resulting from allogenic forcings, like flooding of deltaic surfaces due to RSL rise, can also reduce stratigraphic completeness.

We quantify stratigraphic completeness by calculating the 1-D completeness of all grid nodes in a given stage and then averaging these values to get a representative value for the stage. We start by measuring completeness with  $t$  set to 1 hr, the resolution at which topography was collected. We then analyze the effect of  $t$  on  $C$ . Using our synthetic stratigraphic volumes we proceed by systematically coarsening the temporal resolution from the initial measurement resolution to a final resolution equal to  $0.5T$ , for each stage, by  $\Delta t$  steps of 1 hr. Then for each value of  $t$  we apply Equation 9 to calculate  $C$ . From the resulting plot of  $C$  as a function of  $t$  for each stage (Fig. 16) we make the following observations. 1) As  $t$  increases,  $C$  increases for each stage until saturating at 100%. 2) Over short time scales the control stage has the highest

completeness, followed closely by the LMLP experiment, while the HMSP experiment consistently has the lowest completeness.

## INTERPRETATION

### Flow Confinement and System Mobility

Our results indicate that RSL cycles influence flow confinement and system mobility. Starting with flow confinement, in both the LMLP and HMSP stages we observed a minimum in  $f_w$  during lowstands, while  $f_w$  reached a maximum during highstands (Fig. 7). The reduction of  $f_w$  during lowstands indicates an increase in flow confinement. The stronger response in the HMSP stage is likely associated with the funneling of flow into net incisional channels during periods with high rates of base-level fall. The low magnitude and long period of the sea-level cycles in the LMLP stage, coupled with the long term pseudo-subsidence, meant that RSL never actually decreased in the LMLP stage (Fig. 2). Periods of falling base level in the HMSP stage increased flow confinement as river capture resulted in fewer, but deeper, channels that were more capable of incision.

It is worth noting that while channels did switch to net incision during base-level fall, we did not observe widespread formation of valleys much wider than individual channel threads or regional unconformities in our experiments. This is starkly different from previous experiments that used noncohesive sediment mixtures and produced valleys that rapidly evolved through vertical incision and lateral erosion during periods of base-level fall and rise (Heller et al. 2001; Martin et al. 2011). We note that some modern systems do have strongly cohesive substrates (Stanley et al. 1996) that would reduce incision and lateral erosion rates during base-level fall. It is possible that our experiments are more cohesive, relative to typical shear stresses on the experimental surfaces, than many field-scale systems, while earlier experiments possibly sit at the other end of the cohesion spectrum.

The confinement of flow during lowstands and loss of confinement during highstands also influenced the mobility of the transport systems. Our measurements indicate that the LMLP stage was only slightly more likely to experience topographic modifications at any time, compared to the control stage (Fig. 8). We take this observation as indication that the control and LMLP stages shared similar rates of system mobility. Exploration of time-lapse videos of these stages also supports that they shared similar styles of system mobility, which was dominated by channel avulsion and rapid mobility during channel reorganization phases. In contrast, the fraction of the transport surface modified each hour was higher in the HMSP stage, and this modification was strongly coupled to the position of the shoreline. We interpret this as a signal of lobe deposition as channels end in the sea. During periods of high sea level, locations upstream of the shoreline had high surface-modification values. When coupled to observations from time-lapse photography these high modification values are interpreted as the product of frequent avulsions induced by rapid rates of sea-level rise, which induced in-channel deposition. The opposite is observed in the HMSP-stage during periods of falling sea level, when locations inboard of the shoreline had low values of surface modification interpreted as a result of channel incision.

Finally, the interpreted increase in flow confinement and decrease in lateral mobility as the magnitude of RSL cycles increased can explain why stratigraphic completeness decreased as RSL cycle magnitudes increased (Fig. 16). Flow confinement and reduction in lateral mobility increased time scales of stasis on geomorphic surfaces and aided incision during falling base level, both of which lead to time gaps in stratigraphy.

### Stratigraphic Architecture

Panels of the physical stratigraphy displayed in Figure 10 show significant differences between experimental stages and between the proximal to distal transects. Here, we interpret causes for some of the differences we detailed in the results section. We start with the observation

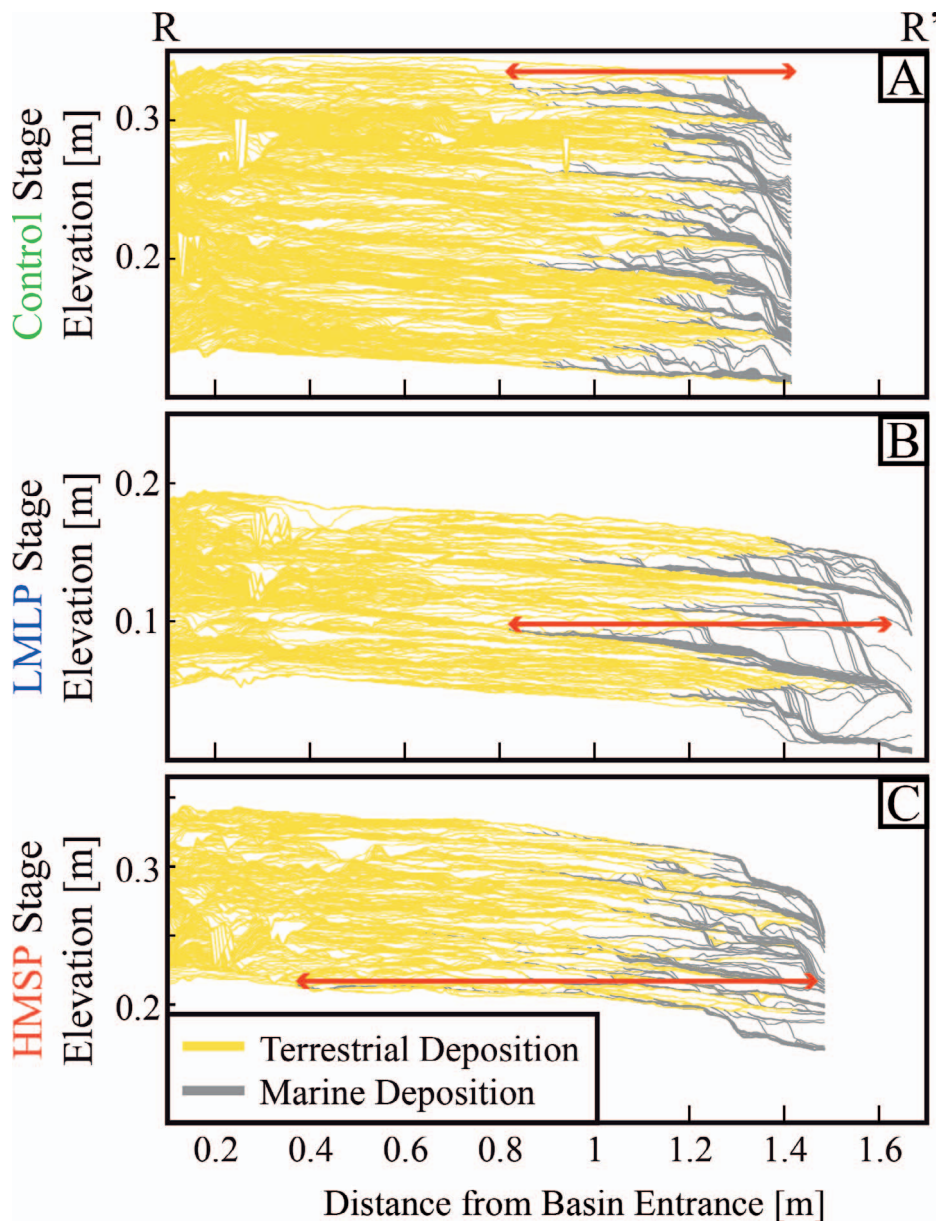


FIG. 12.—Panels of synthetic stratigraphy for a dip transect originating at the basin inlet. A–C) Preserved time lines of the synthetic stratigraphy from the three experimental stages colored by environment of deposition. Red arrows show maximum lateral extent of parasequences in each stage. Location of transect is shown in Figure 13.

that the control stage displays the most well-developed levee deposits. This is interpreted as the consequence of the constant forcings in this stage, which provided no external perturbations to destabilize the transport system. In contrast, the cycles of RSL in the other stages aided the destabilization of channels. This was specifically true during rising RSL when observations and interpretations indicate that in-channel deposition was maximized, leading to channel superelevation and the set-up conditions necessary for channel avulsion.

While some differences are observed in the proximal stratigraphy of the three stages, more pronounced differences are observed in the distal strata from the three stages. The distal strata from the control experiment are composed mainly of coarse terminal lobe deposits separated by thin, fine-grained, and laterally extensive deposits interpreted as condensed sections resulting from autogenic transgressions. By autogenic transgression we mean a transgression driven by shutdown of sediment supply to the shoreline, due to upstream movement of the transport systems through internal processes like avulsions, coupled with background (pseudo)subsidence. These condensed sections result from the bypass of fine-grained

sediment to the sea, which was transported in suspension within the terrestrial channels. This resulted in plumes of fine sediment downstream of the shoreline and aided the construction of prodelta deposits, in addition to the condensed sections in the deltaic stratigraphy. The fraction of the strata composed of coarse sediment decreased in the LMLP stage and further still in the HMSP stage (Fig. 10). We interpret this as the result of more frequent flooding of the coastline due to the allogenicly forced shoreline transgressions. Specifically, the high-magnitude shoreline transgressions in the HMSP stage resulted in large volumes of fine sediment deposited in shallow water depths over most of the delta-top surface. Given the limited lateral mobility of channels during sea-level fall, much of this fine-grained strata was preserved, resulting in relatively small and coarse lobe deposits encased in thick, fine-grained sections. The shoreline transgressions in the HMSP stage extended upstream of the proximal transect location, likely enhancing deposition of fines there as well, which we interpret as the reason why the proximal HMSP strata is finer than the strata of the two other stages. The enhanced proximal deposition of fines in the HMSP stage strata might also result from

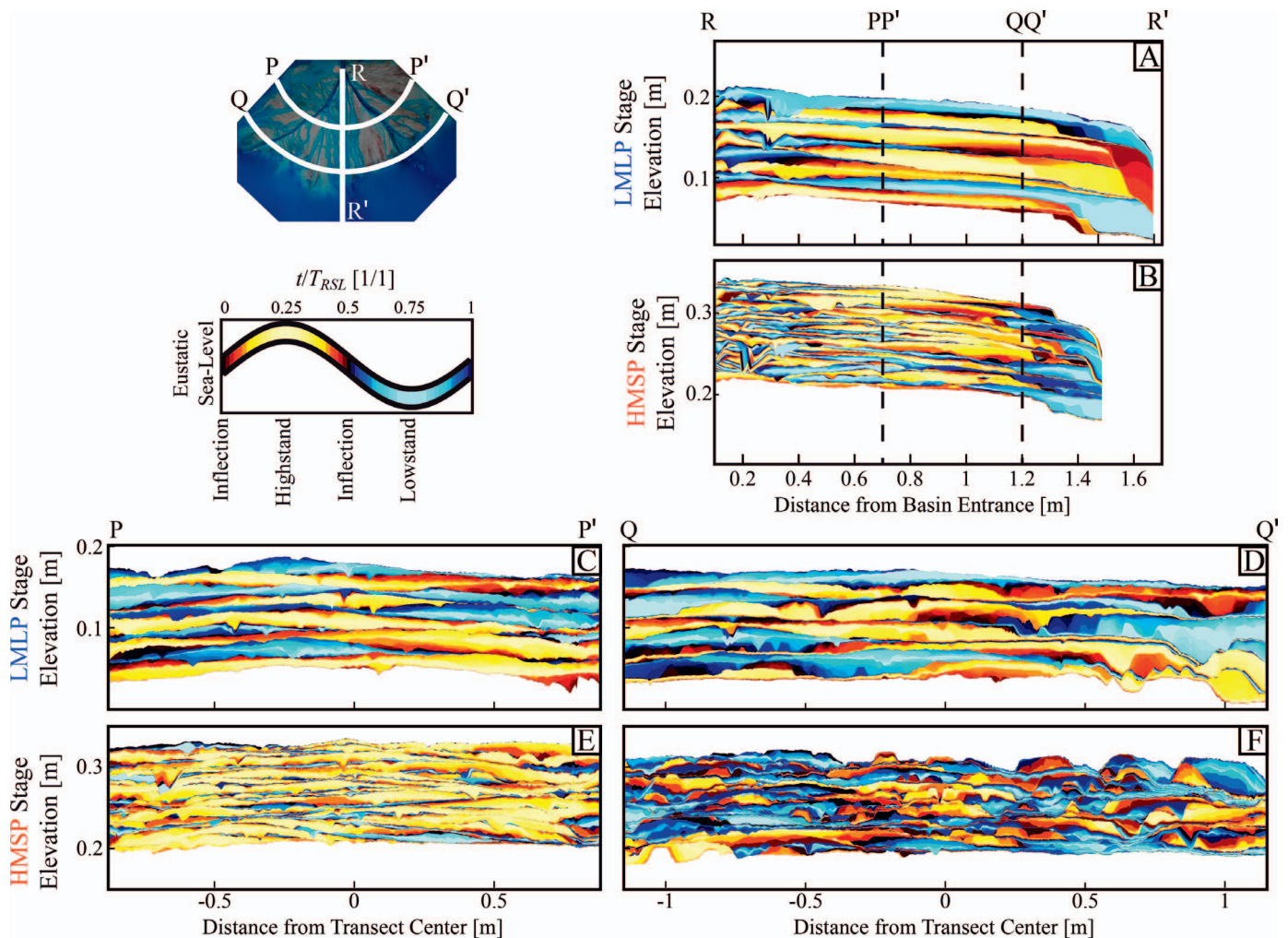


FIG. 13.—Panels of synthetic stratigraphy with deposits painted as a function of time of deposition within a cycle of RSL. Image at top left details location of each transect; color bar details how synthetic stratigraphic color corresponds to time of deposition. Panels include A, B) a dip transect, and C, E) proximal and D, F) distal strike transects.

enhanced bypass of sand-grade material in channels during periods of falling sea level, relative to the control stage.

## DISCUSSION

### Signal Storage in the HMSP vs. LMLP Stages

Analyses detailed in the results and interpretation sections focused on testing our two main hypotheses, which we return to here. The first hypothesis stated that base-level cycles with large magnitudes but short periods induce cyclic morphodynamic responses and produce stratigraphic products with rates and architectural scales that exceed those found in systems with constant forcing. Support for this hypothesis can be found in many of our morphodynamic and stratigraphic results. Starting with shoreline dynamics, we highlight that the shoreline in the HMSP stage was characterized by high migration-rate variability that produced rougher shorelines than observed in either the control or LMLP stages (Figs. 5, 6). This allogenic variability and roughness was maximized during periods of rapid RSL rise as channels on the delta top delivered sediment to the shoreline, which helped counter the shoreline transgressions that occurred at other inactive locations of the delta top. This observation is similar to findings in earlier experimental studies (Kim et al. 2006). In contrast, any allogenic variability in shoreline migration rates and

roughness in the LMLP stage did not rise above the stochastic autogenic signal.

Further morphodynamic support for our first hypothesis can be found in the time–space maps of surface modification (Fig. 8). While the surface-modification maps of the LMLP stage indicate only a slight increase in the fraction of modification per run hour, compared to the control experiment, a clear and strong allogenic signal can be found in the HMSP maps. In the HMSP stage high fractions of surface modification were tied to the position of the shoreline with values that far exceeded the stochastic autogenic values of the control stage. The signal was not restricted to the shoreline, though. During periods of low eustatic sea level, surface-modification fractions inboard of the shoreline were noticeably less than found in the control stage, while periods of high eustatic sea level were associated with surface-modification fractions inboard of the shoreline that were noticeably higher than the control stage.

The allogenic surface dynamics discussed above resulted in stratigraphic attributes that also support our first hypothesis. The frequent and widespread flooding induced by the high-magnitude cycles of the HMSP stage, that were in excess of the autogenic transgressions in the control stage, decreased the fraction of sand stored in its topset stratigraphy relative to the other stages (Fig. 10, 11). Interestingly, in at least one sense the short period of the HMSP RSL cycles resulted in architectural scales less than those found in the control stage. Here we refer to the maximum

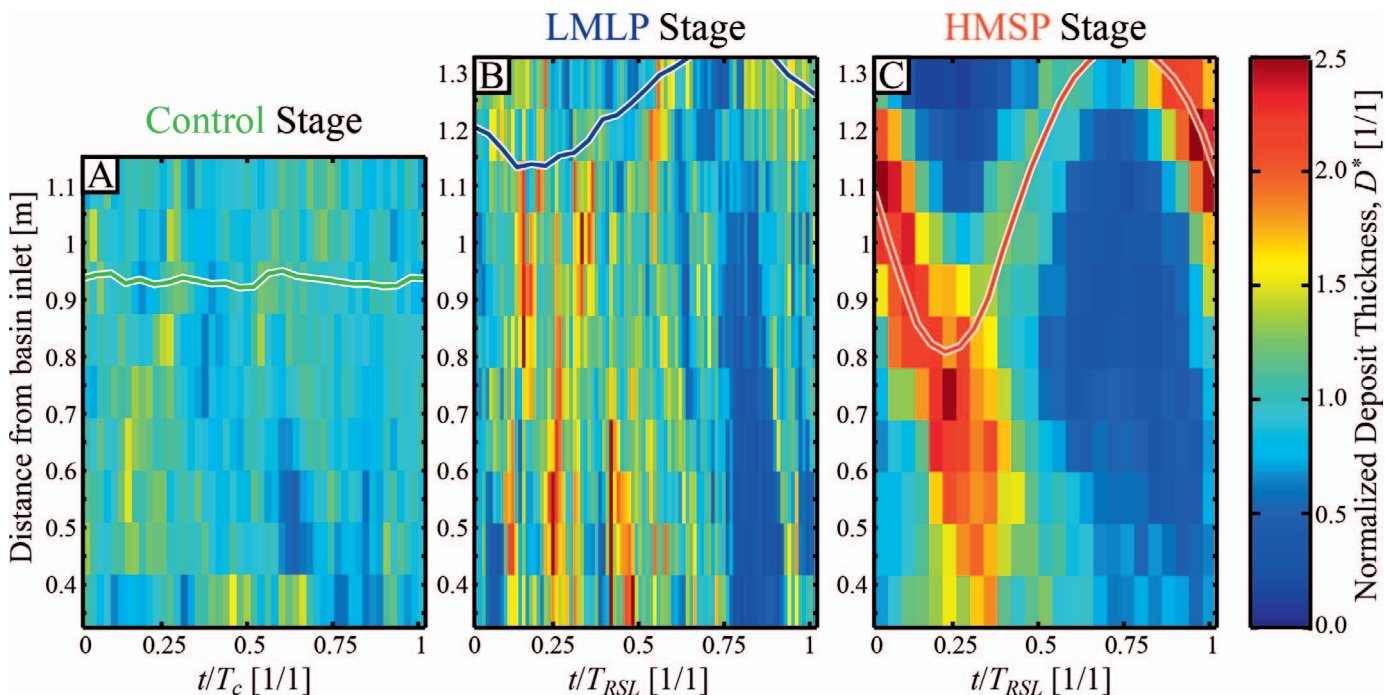


FIG. 14.—Data defining how normalized deposit thickness, resulting from one hour of run time, varies as a function of distance from the basin entrance and time into a sea-level cycle (or cycle of duration  $T_c$  for the control experiment). Thickness is normalized through comparison of pseudo-subsidence generated in one run hour. A–C) Time-space maps of normalized deposit thickness for the control, LMLP, and HMSP stages, respectively. Solid lines within each time-space map indicate the ensemble average location of the shoreline.

thicknesses of parasequences (Fig. 12). In the control stage, parasequences had thicknesses up to the scale of the largest channels and formed over time scales up to  $T_c$ . In the HMSP stage, RSL cycled with a period that was half  $T_c$ . These sea-level cycles forced flooding over most of the delta-top

during highstands, but the short cycles meant that only one-half a channel depth of accommodation was generated by the background pseudo-subsidence over the full cycle. Thus the maximum parasequence thickness was capped at approximately one-half a channel depth. While the allogenic parasequences of the HMSP stage were thinner than the control stage, flooding surfaces in the HMSP stage did extend farther inboard of the mean shoreline than those of the control stage.

The processes associated with parasequence construction highlighted above also resulted in topset strata constructed preferentially, but not exclusively, during sea-level highstands of both the LMLP and HMSP

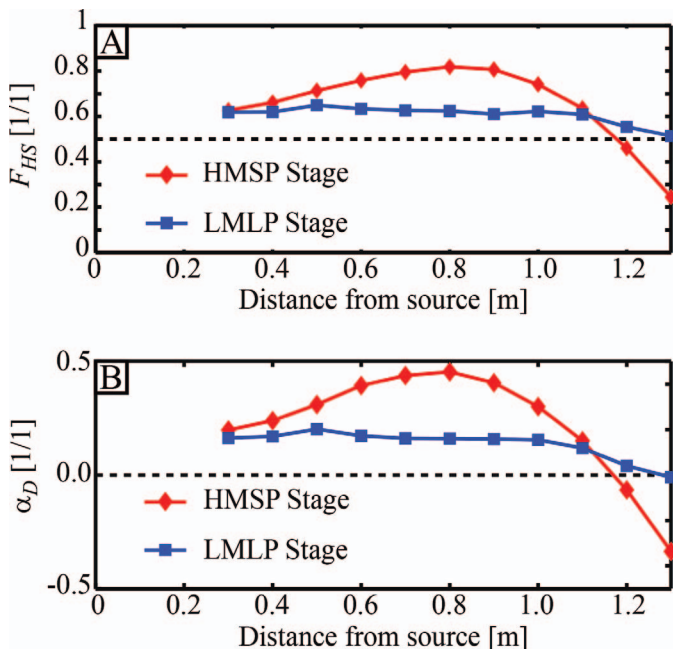


FIG. 15.—Data defining the timing of deposition, within a sea-level cycle, for preserved strata. A) Fraction of strata deposited during highstand conditions as a function of distance from basin entrance. B)  $\alpha_D$  as a function of distance from basin entrance.

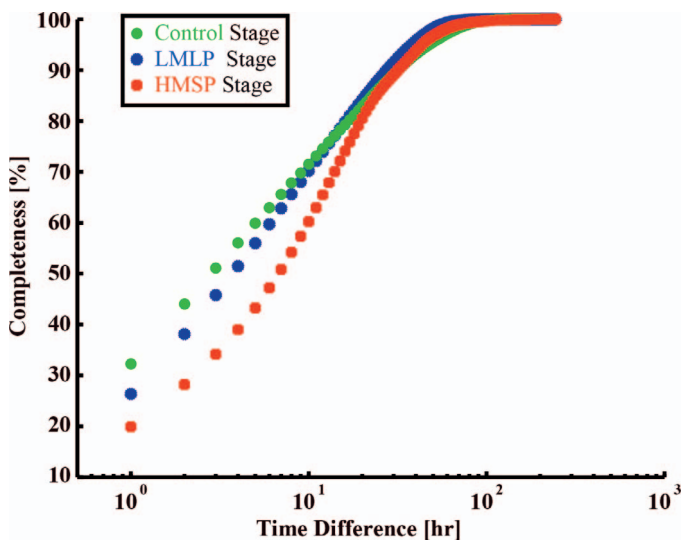


FIG. 16.—Stratigraphic completeness vs. time scale of discretization for the three experimental stages, measured from synthetic stratigraphy.

stages (Figs. 14, 15). Timing and location of deposition was more strongly tied to sea level in the HMSP stage, but we note that even in this stage some deposition occurred during lowstands, in support of recent studies that argue for topset deposition during all phases of sea-level cycles (Schumm 1993; Swenson and Muto 2007; Burgess and Prince 2015; Nijhuis et al. 2015).

The allogenic increase in flow confinement and reduction in system mobility during falling RSL in the HMSP stage also increased periods of stasis on the geomorphic surface relative to the control stage. Enhanced incision during rapid falling of sea level in the HMSP stage also aided removal of sediment from the topset strata. These two processes increased the number and duration of time gaps in the HMSP stage topset strata relative to either the control or LMLP stages. As such extraction of paleo-environmental records from HMSP-influenced deltas will be fairly incomplete, relative to unforced or LMLP systems, at time scales short relative to  $T_c$  (Fig. 16). However, all systems converge to 100% completeness at approximately  $T_c$ . The implication of this analysis is that systems characterized as HMSP will likely have lower temporal fidelity for preserving proxy records of environmental change compared to systems with constant forcings or those that experienced LMLP RSL cycles. We suggest that the data presented, when combined, supports the notion that high-magnitude RSL cycles result in allogenic surface processes and stratigraphic products that are generally higher in magnitude than the autogenic processes and products found in unforced systems.

We now turn our attention to our second hypothesis, that base-level cycles with long periods but small magnitudes will share process rates and stratigraphic architectural scales similar to those of systems with constant forcing. However, these cycles will influence mean attributes of the morphodynamics and store signals of RSL cycles in bulk characteristics of the stratigraphy, e.g., mean volumetric growth rates and mean location of paleo-shoreline indicators, from those in an unforced system. Here we highlight one morphodynamic and one stratigraphic attribute that we suggest support this hypothesis. The morphodynamic result focuses on the location of the mean shoreline (Fig. 6). While the RSL cycles in the LMLP stage did not induce high variability in the migration rate of the shoreline or cause enhanced shoreline roughness, a clear signal can be found in the shoreline position over the course of the ensemble average sea-level cycle. Maximum shoreline transgression occurred during the peak of RSL cycles and maximum regression during the trough of RSL cycles. These shoreline movements change local depositional environments (terrestrial vs. marine) which influence the preservation of attributes from sedimentary structures and fossil type, up to larger-scale stratigraphic architecture.

Movement of the shoreline during the course of a RSL cycle in the LMLP stage did result in a clear stratigraphic signature. Here we refer to the extraction of sediment to the deltaic stratigraphy inboard of the mean shoreline, which was enhanced during periods of highstands (Fig. 9). As a result, local maximum in sediment volume stored inboard of the mean shoreline occurred at the falling inflection of cycles, as eustatic sea level proceeded below its mean value. A signal of this process in the LMLP stage is observed that is of magnitude equal to or slightly higher than that observed in the HMSP stage (Fig. 9D). This result, when viewed in conjunction with our other analyses, suggests that small-magnitude but long-period RSL cycles, as defined by autogenic time and space scales, do little to change the time scales of stochastic deltaic surface processes. However, their long period allows small differences in surface processes, for example the rate of sediment extraction, to compound and produce noticeable differences in the statistics of the final deposit. These results support our second hypothesis.

It is worth highlighting that the clear responses of the mean shoreline (Figs. 5, 6) and sediment extraction inboard of the mean shoreline (Fig. 9), observed in the LMLP stage, are found only after temporally averaging the influence of all five RSL cycles. This averaging process results in response curves for the control experiment that lack structure, while aiding

identification of the response in the LMLP experiment. However, it might be difficult to do this type of averaging for field systems unless stratigraphic age control is available that is linked to knowledge of the timing of RSL cycles. Before temporal averaging, identifying a signal in the raw time series of sediment extraction inboard of the mean shoreline, which differs in magnitude from the stochastic autogenic perturbations found in the control experiment, is difficult. For example, the fourth RSL cycle of the LMLP experiment displays a terrestrial mass-extraction trend opposite to that found in the other four cycles. It appears that the stochasticity in this experiment is large enough to occasionally overprint the forcing signal in the volumetric time series, but not in the ensemble average. This result highlights the need for better theory to define the scales of autogenic perturbations for field systems and further development of techniques to filter these perturbations from field datasets.

While the mass-extraction signature of RSL cycles might require large amounts of chronostratigraphic data, our results on the scales of parasequences hint at possible facies signatures of both the LMLP and HMSP RSL cycles. The parasequences of the control experiment had maximum thicknesses that scaled with the depth of the largest autogenic channels. In addition, as previously noted by Straub et al. (2015), their maximum proximal to distal extent scaled with the system's backwater length,  $L_B$ . The backwater length approximates the distance upstream of the shoreline where channels start to lose sediment transport capacity as their water-surface slopes approach zero to match those of the receiving basin and scales as

$$L_B \approx \frac{H_C}{S} \quad (10)$$

(Chow 1959), where  $S$  is the slope of the transport system. In both the LMLP and HMSP stages the maximum proximal to distal extent of the parasequences exceed  $L_B$ , while parasequence thickness was much greater than  $H_C$  in the LMLP stage and much less than  $H_C$  in the HMSP stage. Estimation of channel depths through preserved channel bodies or complete bar forms (Paola and Borgman 1991; Mohrig et al. 2000) and methods to estimate paleo-slopes (Lynds et al. 2014) provide means to estimate  $H_C$  and  $L_B$  for paleo-systems. As a result, one could compare the lateral extent and thickness of parasequences to the autogenic  $H_C$  and  $L_B$  scales as a means of identification of RSL-cycle signals.

We close this section by noting that the manifestation of the RSL cycles in the HMSP stage is a change in the architecture of the resulting stratigraphy, including the scale of deposit packages. These architectural differences might be detectable with limited time control. However, with the exception of parasequence scales, the manifestation of the RSL cycles in the LMLP experiment was found in more gradually varying parameters, like the extraction of mass from transport. These signals might require precise geochronological control to observe in field-scale stratigraphy.

### Large and/or Long RSL Cycles in Field-Scale Systems

Given our discussion of the morphodynamic and stratigraphic attributes of RSL cycles, when normalized by autogenic temporal and spatial scale, an obvious question is where and when might we expect to find either LMLP or HMSP systems. To address this, we use a database of modern systems where information concerning  $H_c$  and  $T_c$  were compiled. This database was first presented by Li et al. (2016), who visualized the information in a slightly different way than presented here.  $T_c$  was estimated for these systems using information compiled on the long-term aggradation rates of systems and the relationship:

$$T_c = \frac{H_c}{\bar{r}} \quad (11)$$

(Wang et al. 2011).  $H_c$  and  $T_c$  are then compared to Milankovitch-scale RSL cycles in the middle Pleistocene to the present when eccentricity

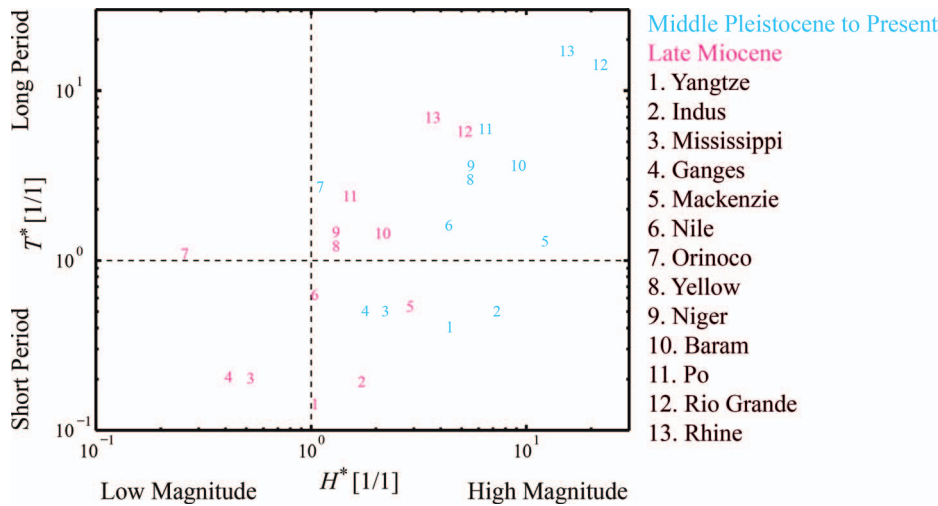


FIG. 17.—Predictions of magnitude and period of RSL cycles when normalized by autogenic length and time scales for 13 major river systems. Data were originally published by Li et al. (2016). Predictions are for two time periods, the middle Pleistocene to the present (cyan) and the late Miocene (magenta) and are based on modern channel depths and long term (time window of measurement > 100 ky) sedimentation rates.

cycles (~ 100 ky) resulted in RSL changes of ~ 100 m and late Miocene conditions when obliquity cycles (~ 40 ky) resulted in RSL changes with ranges of 10–35 m. Similarly to Li et al., we highlight that  $H_c$  values in our database are constructed from modern channel depths and we acknowledge that some change in channel depths have occurred since the late Miocene due to changing boundary conditions. However, these changes are unlikely to influence the general observations highlighted below. These comparisons are made quantitatively with Equations 2 and 3 and shown in Figure 17. With this compilation we make the following observations. Given the high magnitude of middle Pleistocene to present eccentricity cycles, all systems in our database for this time are characterized by  $H^*$  values in excess of one. Between the middle Pleistocene to the present many of these systems are also characterized by high  $T^*$  values. Thus, some but not all systems in our database can be characterized as HMSP during the middle Pleistocene to the present.

The smaller amplitude of RSL cycles in the late Miocene reduces the  $H^*$  of systems in our database, but associated with this is a decrease in  $T^*$  as the late Miocene was dominated by shorter-duration obliquity cycles. As a result, we again observe some HMSP and high-magnitude, long-period systems during the late Miocene, but no systems that confidently fall within the LMLP quadrant. This leads to the question: do the scales of sea-level cycles commonly attributed to Milankovitch forcing ever lead to LMLP RSL deltaic systems? While not included in our database, several observations from the literature suggest that this might be possible. Examination of Equations 2, 3, and 11 indicate that the following conditions are necessary to produce a LMLP RSL-cycle system. First, deep channels aid the ability to get low  $H^*$  values from small-magnitude cycles. Second, basins with high subsidence rates help decrease  $T_c$  and thus help increase  $T^*$ .

Candidate systems which could fulfill the conditions outlined above include 1) the Fish Creek–Vallecito Basin, filled by the paleo–Colorado River delta. Deltaic stratigraphy, imaged in outcrops from this basin and deposited 4–5 Ma, have dune cross bedding with scales up to 10 m (Dorsey, personal communication), which could indicate channel depths up to 30 m (Paola and Borgman 1991). In addition, basin subsidence rates were exceptionally high, with sustained rates up to 2.2 mm/yr (Dorsey et al. 2011). These values and characteristic eustatic cycles during this time (Miller et al. 2005) suggest  $H^*$  and  $T^*$  values of approximately 0.5 and 2, respectively.

Additional LMLP candidate systems might exist in the Cretaceous stratigraphy of large-river delta systems. The Cretaceous exemplifies greenhouse Earth conditions, when limited or no continental-scale glaciers existed, which reduced the magnitude of RSL cycles. Some studies suggest

that RSL cycles were as long as 100 or 300 ky during this period (Haq 2014); however, the record of sea-level at this time contains large uncertainty. As a result, systems of a Mississippi River Delta scale or larger during this time might be characterized as LMLP. Again, we note that our results suggest that stratigraphic evidence from these systems that would indicate their forcing by LMLP RSL cycles, might necessitate high-precision geochronology data.

SUMMARY

The work detailed above builds on a long history of investigation into the influence of RSL cycles on deltaic surface processes and stratigraphic products. Here, we specifically build on the work of Li et al. (2016), who first presented the approach to normalize the magnitude and period of RSL cycles by deltaic autogenic time and space scales. The goal of this paper was to document how surface processes and stratigraphic products vary in experimental deltas that experience either high-magnitude but short-period or low-magnitude but long-period RSL cycles, as normalized by autogenic space and time scales. Exploration of surface processes focused on those with clear links to the preserved stratigraphic record. The main results are summarized as follows:

Our analysis indicates that the response of deltas to HMSP RSL cycles can be found in periodic morphodynamic processes with rates and scales that exceed the stochastic autogenic variability found in systems with constant forcings. These morphodynamics produce stratigraphic attributes that are significantly different from autogenic stratigraphy. Specifically, we find that HMSP RSL cycles result in deltas with spatially variable shoreline migration rates that yield rough shorelines. These cycles induce significant reductions in system mobility during lowstands and enhance mobility during highstands. Over the course of a full cycle, the high magnitude aids retention of fines in delta-top stratigraphy and reduces the thickness of parasequences compared to autogenic systems. Finally, their topset stratigraphy is preferentially, but not exclusively, constructed during highstands.

The morphodynamic and stratigraphic response to the LMLP cycles was more subtle. Stochastic attributes of the surface processes, for example variability in shoreline migration rates, were only slightly different from the control experiment. However, the long period of these cycles allowed small differences to sum together to give clear signals in attributes like the mean shoreline location or the mass extraction inboard of the mean shoreline. We suggest that the recognition of cycles in deposition or volumetric growth rates in field-scale stratigraphy might be challenging due to limited architectural differences relative to constantly forced

systems, but high precision geochronology might aid signal extraction of volumetric growth rates.

Analysis of channel depths and long-term sedimentation rates from 13 major river deltas suggest that commonly discussed Milankovitch-scale eustatic sea-level cycles during both the late Miocene and the middle Pleistocene to the present are frequently of high magnitude but short period compared to autogenic scales. While the dominant periodicity of sea-level cycles in either the Quaternary or the late Miocene are not felt as low magnitude and long periodicity by the systems in our database, some evidence from earlier studies suggest that these types of cycles might have existed in the past.

#### ACKNOWLEDGMENTS

This study was supported by the National Science Foundation (grant EAR-1424312), a graduate student research grant from the Geological Society of America, and a summer research award from Schlumberger. We thank the members of the Tulane Sediment Dynamics and Stratigraphy Lab for help with the experiments. Data used in this study can be found at the SEAD online data repository (Li and Straub 2017; Yu and Straub 2017). Finally, we thank Robert Duller and Peter Burgess for reviews that strengthened the manuscript and for technical edits from John Southard.

Li, Q., and Straub, K.M., 2017, TDB\_12\_1, SEAD, <http://doi.org/10.5967/M03N21GX>.

Yu, L., and Straub, K.M., 2017, TDB\_15\_1, SEAD, <http://doi.org/10.5967/M00V89W1>.

#### REFERENCES

- AGER, D.V., 1973, *The Nature of the Stratigraphic Record*, Wiley, 114 p.
- ANDERSON, J.B., 2004, Late Quaternary stratigraphic evolution of the northern Gulf of Mexico margin: a synthesis, in Anderson, J.B., and Fillon, R.H., eds., *Late Quaternary Stratigraphic Evolution of the Northern Gulf of Mexico Margin*: SEPM, Special Publication 79, p. 1–23.
- BHATTACHARYA, J.P., 2011, Practical problems in the application of the sequence stratigraphic method and key surfaces: integrating observations from ancient fluvial–deltaic wedges with Quaternary and modelling studies: *Sedimentology*, v. 58, p. 120–169.
- BLUM, M.D., AND TÖRNQVIST, T.E., 2000, Fluvial responses to climate and sea-level change: a review and look forward: *Sedimentology*, v. 47, p. 2–48.
- BURGESS, P.M., AND PRINCE, G.D., 2015, Non-unique stratigraphic geometries: implications for sequence stratigraphic interpretations: *Basin Research*, v. 27, p. 351–365.
- CATUNEANU, O., 2002, Sequence stratigraphy of clastic systems: concepts, merits, and pitfalls: *Journal of African Earth Sciences*, v. 35, p. 1–43.
- CATUNEANU, O., ABREU, V., BHATTACHARYA, J.P., BLUM, M.D., DALRYMPLE, R.W., ERIKSSON, P.G., FIELDING, C.R., FISHER, W.L., GALLOWAY, W.E., GIBLING, M.R., GILES, K.A., HOLBROOK, J.M., JORDAN, R., KENDALL, C.G.S.C., MACURDA, B., MARTINSEN, O.J., MIALL, A.D., NEAL, J.E., NUMMEDAL, D., POMAR, L., POSAMENTIER, H.W., PRATT, B.R., SARG, J.F., SHANLEY, K.W., STEEL, R.J., STRASSER, A., TUCKER, M.E., AND WINKER, C., 2009, Towards the standardization of sequence stratigraphy: *Earth-Science Reviews*, v. 92, p. 1–33.
- CAZANACLI, D., PAOLA, C., AND PARKER, G., 2002, Experimental steep, braided flow: application to flooding risk on fans: *Journal of Hydraulic Engineering*, v. 128, p. 322–330.
- CHAMBERLIN, E.P., AND HAJEK, E.A., 2015, Interpreting paleo-avulsion dynamics from multistory sand bodies: *Journal of Sedimentary Research*, v. 85, p. 82–94.
- CHOW, V.T., 1959, *Open-Channel Hydraulics*: New York, McGraw-Hill, 680 p.
- DALMAN, R., WELTJE, G.J., AND KARAMITPOULOS, P., 2015, High-resolution sequence stratigraphy of fluvio–deltaic systems: prospects of system-wide chronostratigraphic correlation: *Earth and Planetary Science Letters*, v. 412, p. 10–17.
- DORSEY, R.J., HOUSEN, B.A., JANECKE, S.U., FANNING, C.M., AND SPEARS, A.L., 2011, Stratigraphic record of basin development within the San Andreas fault system: late Cenozoic Fish Creek–Vallecito basin, southern California: *Geological Society of America, Bulletin*, v. 123, p. 771–793.
- FLEMINGS, P.B., AND GROTZINGER, J.P., 1996, STRATA: Freeware for analyzing classic stratigraphic problems: *GSA Today*, v. 6, p. 1–7.
- GILBERT, G.K., 1890, *Lake Bonneville*: Washington, D.C., U.S. Government Printing Office, U.S. Geologic Survey, Monograph 1, 438 p.
- GRANJEON, D., AND JOSEPH, P., 1999, Concepts and applications of a 3-D multiple lithology, diffusive model in stratigraphic modeling, in Harbaugh, J.W., Watney, W.L., Rankey, E.C., Slingerland, R., and Goldstein, R.H., eds., *Numerical Experiments in Stratigraphy*: SEPM, Special Publication 62, p. 197–210.
- HAJEK, E.A., HELLER, P.L., AND SCHUR, E.L., 2012, Field test of autogenic control on alluvial stratigraphy (Ferris Formation, Upper Cretaceous–Paleogene, Wyoming): *Geological Society of America, Bulletin*, v. 124, p. 1898–1912.
- HAQ, B.U., 2014, Cretaceous eustasy revisited: *Global and Planetary Change*, v. 113, p. 44–58.
- HELLER, P.L., PAOLA, C., HWANG, I., JOHN, B., AND STEEL, R., 2001, Geomorphology and sequence stratigraphy due to slow and rapid base-level changes in an experimental subsiding basin (XES 96-1): *American Association of Petroleum Geologists, Bulletin*, v. 85, p. 817–838.
- HICKSON, T.A., SHEETS, B.A., PAOLA, C., AND KELBERER, M., 2005, Experimental test of tectonic controls on three-dimensional alluvial facies architecture: *Journal of Sedimentary Research*, v. 75, p. 710–722.
- HOFMANN, M.H., WROBLEWSKI, A., AND BOYD, R., 2011, Mechanisms controlling the clustering of fluvial channels and the compensational stacking of cluster belts: *Journal of Sedimentary Research*, v. 81, p. 670–685.
- HOYAL, D.C.J.D., AND SHEETS, B.A., 2009, Morphodynamic evolution of experimental cohesive deltas: *Journal of Geophysical Research, Earth Surface*, v. 114, no. F02009.
- KARAMITPOULOS, P., WELTJE, G.J., AND DALMAN, R., 2014, Allogenic controls on autogenic variability in fluvio-deltaic systems: inferences from analysis of synthetic stratigraphy: *Basin Research*, v. 26, p. 767–779.
- KARSENBERG, D., AND BRIDGE, J.S., 2008, A three-dimensional numerical model of sediment transport, erosion and deposition within a network of channel belts, floodplain and hill slope: extrinsic and intrinsic controls on floodplain dynamics and alluvial architecture: *Sedimentology*, v. 55, p. 1717–1745.
- KIM, W., AND PAOLA, C., 2007, Long-period cyclic sedimentation with constant tectonic forcing in an experimental relay ramp: *Geology*, v. 35, p. 331–334.
- KIM, W., PAOLA, C., SWENSON, J.B., AND VOLLER, V.R., 2006, Shoreline response to autogenic processes of sediment storage and release in the fluvial system: *Journal of Geophysical Research, Earth Surface*, v. 111, no. F04013.
- KIM, W., SHEETS, B., AND PAOLA, C., 2010, Steering of experimental channels by lateral basin tilting: *Basin Research*, v. 22, p. 286–301.
- KOSS, J.E., ETHRIDGE, F.G., AND SCHUMM, S.A., 1994, An experimental study of the effects of base-level change on fluvial, coastal-plain, and shelf systems: *Journal of Sedimentary Research*, v. 64, p. 90–98.
- LI, Q., YU, L., AND STRAUB, K.M., 2016, Storage thresholds for relative sea-level signals in the stratigraphic record: *Geology*, v. 44, p. 179–182.
- LIANG, M., VAN DYK, C., AND PASSALACQUA, P., 2016, Quantifying the patterns and dynamics of river deltas under conditions of steady forcing and relative sea level rise: *Journal of Geophysical Research, Earth Surface*, v. 121, p. 465–496.
- LYNDS, R.M., MOHRIG, D., HAJEK, E.A., AND HELLER, P.L., 2014, Paleoslope reconstruction in sandy suspended-load-dominant rivers: *Journal of Sedimentary Research*, v. 84, p. 825–836.
- MACKIN, J.H., 1948, Concept of the graded river: *Geological Society of America, Bulletin*, v. 59, p. 463–512.
- MARTIN, J., PAOLA, C., ABREU, V., NEAL, J., AND SHEETS, B., 2009, Sequence stratigraphy of experimental strata under known conditions of differential subsidence and variable base level: *American Association of Petroleum Geologists, Bulletin*, v. 93, p. 503–533.
- MARTIN, J., CANTELLI, A., PAOLA, C., BLUM, M., AND WOLINSKY, M., 2011, Quantitative modeling of the evolution and geometry of incised valleys: *Journal of Sedimentary Research*, v. 81, p. 64–79.
- MILLER, K.G., KOMINZ, M.A., BROWNING, J.V., WRIGHT, J.D., MOUNTAIN, G.S., KATZ, M.E., SUGARMAN, P.J., CRAMER, B.S., CHRISTIE-BLICK, N., AND PEKAR, S.F., 2005, The Phanerozoic record of global sea-level change: *Science*, v. 310, p. 1293–1298.
- MOHRIG, D., HELLER, P.L., PAOLA, C., AND LYONS, W.J., 2000, Interpreting avulsion process from ancient alluvial sequences: Guadalupe–Matarranya (northern Spain) and Wasatch Formation (western Colorado): *Geological Society of America Bulletin*, v. 112, p. 1787–1803.
- MUTO, T., 2001, Shoreline autoretreat substantiated in flume experiments: *Journal of Sedimentary Research*, v. 71, p. 246–254.
- NIJHUIS, A., EDMONDS, D., CALDWELL, R., CEDERBERG, J., SLINGERLAND, R., BEST, J., PARSONS, D., AND ROBINSON, R., 2015, Fluvio-deltaic avulsions during relative sea-level fall: *Geology*, v. 43, p. 719–722.
- PAOLA, C., AND BORGMAN, L., 1991, Reconstructing random topography from preserved stratification: *Sedimentology*, v. 38, p. 553–565.
- PAOLA, C., HELLER, P.L., AND ANGEVINE, C.L., 1992, The large-scale dynamics of grain-size variation in alluvial basins, I: Theory: *Basin Research*, v. 4, p. 73–90.
- POSAMENTIER, H.W., AND VAIL, P.R., 1988, Eustatic controls on clastic deposition II: sequence and systems tract models, in Wilgus, C.K., Hastings, B.S., Posamentier, H.P., Van Wagoner, J.V., Ross, C.A., and Kendall, C.G.S.C., eds., *Sea-Level Changes: An Integrated Approach*: SEPM, Special Publication 42, p. 125–154.
- SADLER, P.M., AND STRAUSS, D.J., 1990, Estimation of completeness of stratigraphical sections using empirical data and theoretical models: *Geological Society of London, Journal*, v. 147, p. 471–485.
- SCHUMM, S., 1993, River response to base-level change: implications for sequence stratigraphy: *The Journal of Geology*, v. 101, p. 279–294.
- STANLEY, D.J., WARNE, A.G., AND DUNBAR, J.B., 1996, Eastern Mississippi delta: late Wisconsin unconformity, overlying transgressive facies, sea level and subsidence: *Engineering Geology*, v. 45, p. 359–381.

- STRAUB, K.M., AND ESPOSITO, C.R., 2013, Influence of water and sediment supply on the stratigraphic record of alluvial fans and deltas: process controls on stratigraphic completeness: *Journal of Geophysical Research, Earth Surface*, v. 118, p. 1–13.
- STRAUB, K.M., AND WANG, Y., 2013, Influence of water and sediment supply on the long-term evolution of alluvial fans and deltas: statistical characterization of basin-filling sedimentation patterns: *Journal of Geophysical Research, Earth Surface*, v. 118, p. 1–15.
- STRAUB, K.M., LI, Q., AND BENSON, W.M., 2015, Influence of sediment cohesion on deltaic shoreline dynamics and bulk sediment retention: a laboratory study: *Geophysical Research Letters*, v. 42, p. 9808–9815.
- SWENSON, J.B., AND MUTO, T., 2007, Response of coastal plain rivers to falling relative sea-level: allogenic controls on the aggradational phase: *Sedimentology*, v. 54, p. 207–221.
- TRAMPUSH, S., HAJEK, E., STRAUB, K., AND CHAMBERLIN, E., 2017, Identifying autogenic sedimentation in fluvial-deltaic stratigraphy: evaluating the effect of outcrop-quality data on the compensation statistic: *Journal of Geophysical Research, Earth Surface*, v. 122, p. 1–23.
- VAIL, P.R., 1987, Seismic stratigraphy interpretation utilizing sequence stratigraphy Part 1: seismic stratigraphy interpretation procedure, in Bally, W.W., ed., *Atlas of Seismic Stratigraphy*: American Association of Petroleum Geologists, *Studies in Geology*, p. 1–10.
- VAIL, P.R., MITCHUM, R.M., AND THOMPSON, S., 1977, Seismic stratigraphy and global changes of sea level, Part 4: global cycles of relative changes of sea level, in Payton, C.E., ed., *Seismic Stratigraphy: Applications to Hydrocarbon Exploration*: American Association of Petroleum Geologists, *Memoir* 26, p. 83–98.
- VAN DIJK, M., POSTMA, G., AND KLEINHANS, M.G., 2009, Autocyclic behaviour of fan deltas: an analogue experimental study: *Sedimentology*, v. 56, p. 1569–1589.
- VAN HEIJST, M.W.L.M., AND POSTMA, G., 2001, Fluvial response to sea-level changes: a quantitative analogue, experimental approach: *Basin Research*, v. 13, p. 269–292.
- VAN WAGONER, J.C., MITCHUM, R.M., CAMPION, K.M., AND RAHMANIAN, V.D., 1990, Siliciclastic Sequence Stratigraphy in Well Logs, Cores, and Outcrops: Concepts for High-Resolution Correlation of Time and Facies: *American Association of Petroleum Geologists, Methods in Exploration* 7, 55 p.
- WANG, Y., STRAUB, K.M., AND HAJEK, E.A., 2011, Scale-dependent compensational stacking: an estimate of autogenic time scales in channelized sedimentary deposits: *Geology*, v. 39, p. 811–814.
- WOOD, L.J., ETHRIDGE, F.G., AND SCHUMM, S.A., 1993, The effects of rate of base-level fluctuation on coastal-plain, shelf and slope depositional systems: an experimental approach, in Posamentier, H.W., Summerhayes, C.P., Haq, B.U., and Allen, G.P., eds., *Sequence Stratigraphy and Facies Associations*: International Association of Sedimentologists, *Special Publication* 18, p. 43–53.
- ZECCHIN, M., AND CATUNEANU, O., 2013, High-resolution sequence stratigraphy of clastic shelves I: units and bounding surfaces: *Marine and Petroleum Geology*, v. 39, p. 1–25.

Received 27 December 2016; accepted 22 May 2017.